

# HADRONIC PARITY VIOLATION: A New View Through the Looking Glass

---

Michael J. Ramsey-Musolf

*Kellogg Radiation Laboratory, California Institute of Technology, Pasadena, California  
91125; e-mail: mjrm@caltech.edu*

Shelley A. Page

*Department of Physics and Astronomy, University of Manitoba, Winnipeg, Manitoba,  
R3T 2N2 Canada; e-mail: spage@cc.umanitoba.ca*

**Key Words** hadronic weak interaction, nuclear parity violation, effective field theory

■ **Abstract** Studies of the strangeness-changing hadronic weak interaction have produced a number of puzzles that have evaded a complete explanation within the Standard Model. Their origin may lie either in dynamics peculiar to weak interactions involving strange quarks or in more general aspects of the interplay between strong and weak interactions. In principle, studies of the strangeness-conserving hadronic weak interaction using parity-violating hadronic and nuclear observables provide a complementary window to this question. However, progress in this direction has been hampered by the lack of a suitable theoretical framework for interpreting hadronic parity violation measurements in a model-independent way. Recent work involving effective field theory ideas has led to the formulation of such a framework, simultaneously motivating the development of a number of new hadronic parity violation experiments in few-body systems. We review these recent developments and discuss the prospects and opportunities for further experimental and theoretical progress.

## CONTENTS

1. INTRODUCTION .....	2
2. WEAK MESON-EXCHANGE MODEL MEETS THE END OF THE ROAD .....	6
2.1. Meson-Exchange Model of the Weak Nucleon-Nucleon Interaction .....	7
2.2. Experimental Progress .....	12
2.3. The End of the Road .....	23
3. EFFECTIVE FIELD THEORY FRAMEWORK .....	25
3.1. The Pionless Effective Field Theory .....	26
3.2. Parity-Violating Effective Field Theory with Pions .....	32
3.3. Recent Theoretical Work .....	39
3.4. Experimental Prospects .....	44

4. BEYOND HADRONIC PARITY VIOLATION .....	47
5. SUMMARY AND CONCLUSIONS .....	48

## 1. INTRODUCTION

Explaining the weak interactions of quarks in terms of the dynamics of the Standard Model (SM) has been an area of vigorous research in nuclear and particle physics for several decades. Experimentally, the hadronic weak interaction (HWI) is probed by observing nonleptonic, flavor-changing decays of mesons and baryons and by measuring observables that conserve flavor but violate the parity symmetry of the strong and electromagnetic (EM) interactions. Theoretically, the problem has been particularly challenging, requiring the computation of low-energy weak matrix elements of the HWI in strongly interacting systems. Although the structure of the weak quark-quark interaction in the SM has been well established for some time, its manifestation in strongly interacting systems remains only partially understood. The stumbling block has been the nonperturbative nature of quantum chromodynamics (QCD) at low energies. In contending with it, theorists have resorted to a variety of approximation schemes to obtain physically reasonable estimates of HWI observables. Ultimately, however, arriving at definitive SM predictions requires a rigorous treatment of nonperturbative QCD dynamics.

In the case of the flavor-changing decays of mesons, use of effective field theory (EFT) techniques—chiral perturbation theory ( $\chi$ PT), heavy-quark effective theory, and recently, soft-collinear effective theory—has led to enormous progress. In each instance, the presence of distinct physical scales at play in the processes of interest allows for a systematic expansion of the effective Lagrangian in powers of scale ratios, while incorporating the symmetries of QCD into the structure of the operators. The operator coefficients that encode the nonperturbative QCD dynamics are obtained from measurement, and the structure of the EFT is then used to translate this information into predictions for other observables. Moreover, physicists can make a meaningful confrontation of experiment with QCD theory, as computations of the operator coefficients can in principle be performed on the lattice.

The situation involving the HWI of baryons is far less satisfactory, and decades of experimental and theoretical work have left physicists with a number of unresolved puzzles. In the case of hyperon nonleptonic decays, for example, physicists have not yet achieved a simultaneous accounting for both the parity-conserving P-wave and parity-violating (PV) S-wave decay amplitudes. Similarly, some PV asymmetries associated with the radiative decays of hyperons are anomalously large. In the limit of degenerate  $u$ -,  $d$ -, and  $s$ -quarks, SU(3) flavor symmetry implies that these asymmetries must vanish. Given the known mass splitting between the strange and two light flavors, the asymmetries should have magnitudes of order  $m_s/M_B \sim 0.15$ , where  $M_B \sim 1$  GeV is a typical hyperon mass. The experimental asymmetries, in contrast, are four to five times larger in magnitude. Even the well-known  $\Delta I = 1/2$  rule that summarizes the observed dominance of the  $I = 1/2$  channel over the  $I = 3/2$  channel in strangeness-changing nonleptonic decays

remains enigmatic, as no apparent symmetry favors either channel. In short, consideration of QCD symmetries and the relevant physical scales still does not account for the observed properties of the  $\Delta S = 1$  HWI.

Although the puzzles surrounding the strangeness-changing HWI have been discussed extensively elsewhere, the  $\Delta S = 0$  HWI has in general received less attention. Nonetheless, because we do not know whether the breakdown of QCD symmetry-based expectations in the  $\Delta S = 1$  sector results from the presence of a dynamical strange quark or from other, yet-to-be-uncovered dynamics, consideration of the  $\Delta S = 0$  HWI—for which the strange quark plays a relatively minor role—is no less important. We focus on this component of the HWI below.

According to the SM, the structure of the low-energy  $\Delta S = 0$  HWI is relatively simple:

$$\mathcal{H}_{\text{HWI}}^{\Delta S=0} = \frac{G_F}{\sqrt{2}} \left( J_\lambda^{CC\dagger} J^{\lambda CC} + \frac{1}{2} J_\lambda^{NC\dagger} J^{\lambda NC} \right), \quad 1.$$

where  $G_F$  is the Fermi constant and  $J_\lambda^{CC}$  and  $J_\lambda^{NC}$  are the weak charged and neutral currents, respectively. The theoretical challenge is to find the appropriate effective interaction  $\mathcal{H}_{\text{HWI}}^{\Delta S=0 \text{ eff}}(N, \pi, \Delta, \dots)$  that best describes the hadronic manifestation of  $\mathcal{H}_{\text{HWI}}^{\Delta S=0}$ . Because  $J_\lambda^{CC}$  transforms as a doublet under strong isospin, whereas  $J_\lambda^{NC}$  contains  $I = 0$  and  $I = 1$  components, the current-current products in  $\mathcal{H}_{\text{HWI}}^{\Delta S=0}$  contain terms that transform as isoscalars, isovectors, and isotensors. Consequently,  $\mathcal{H}_{\text{HWI}}^{\Delta S=0 \text{ eff}}$  must contain the most general set of operators having the same isospin properties. Below, we review the theoretical efforts to determine this effective interaction.

Experimentally, the  $\Delta S = 0$  HWI can be isolated solely via hadronic and nuclear physics processes that violate parity, thereby filtering out the much larger effects of the strangeness-conserving strong and EM interactions. Efforts to do so are not new. Soon after the 1957 discovery of parity violation in  $\mu$ -decay and nuclear  $\beta$ -decay, the search was on for evidence of a PV weak nuclear force that would result in small PV effects in nuclear observables. That year, Tanner (1) reported the first experimental search for a PV nucleon-nucleon (NN) interaction. Subsequently, Feynman & Gell-Mann (2) predicted that the four fermion interactions responsible for leptonic and semileptonic weak decays should have a four-nucleon partner that is similarly first order in  $G_F$ . A decade later, Lobashov et al. (3, 4) produced the first definitive evidence for the existence of a first order, weak NN force in radiative neutron capture on  $^{181}\text{Ta}$  consistent with the Feynman & Gell-Mann hypothesis.

The pursuit of this evidence in the Tanner, Lobashov, and subsequent experiments was challenging, as the magnitude of the PV effects was expected to be  $\mathcal{O}(10^{-7})$ . Along the way, physicists realized that certain accidents of nuclear structure in many-body nuclei could amplify the expected PV effects by several orders of magnitude, and a  $\sim 10\%$  PV effect was indeed observed in  $^{139}\text{La}$  (5). The amplification arises from two sources: the presence of nearly degenerate opposite-parity states that are mixed by the HWI, and the interference of an otherwise parity-forbidden transition amplitude with a much larger parity-allowed one. Subsequent

experiments yielded a mix of PV measurements in nuclei in which amplification factors of order  $10^2$  to  $10^3$  were expected, as well as studies of PV observables in the scattering of polarized protons and neutrons from hadronic targets.

Theoretically, however, the use of nuclear systems introduces an additional level of complication in the interpretation of experiments as one must contend with both nuclear structure effects as well as the dynamics of nonperturbative QCD. For more than two decades the conventional framework for carrying out this interpretation has been a meson-exchange model, popularized by the seminal work of Desplanques, Donoghue & Holstein (DDH) (6). The model assumes that the PV NN interaction is dominated by the exchange of the pion and the two lightest vector mesons ( $\rho$  and  $\omega$ ) and that its strength is characterized by seven PV meson-nucleon couplings:  $h_\pi^1$ ,  $h_\rho^{0,1,2}$ ,  $h_\rho^V$ , and  $h_\omega^{0,1}$ , where the superscript indicates the isospin.<sup>1</sup> DDH provided theoretical “reasonable ranges” and “best values” for the  $h_M^i$  using SU(6) symmetry, constraints from nonleptonic hyperon decay data, and the quark model to estimate the experimentally unconstrained terms. Despite various attempts to improve upon the original DDH work, the results of their analysis still remain the benchmark theoretical targets for the PV meson-nucleon couplings.

The experimental results from nuclear and hadronic PV measurements have been analyzed using the DDH framework, leading to constraints on combinations of the  $h_M^i$  that typically enter PV observables. The results agree in general with the DDH reasonable ranges, although the ranges themselves are quite broad and the constraints from different experiments are not entirely consistent. A particular quandary involves  $h_\pi^1$ : The  $\gamma$ -decays of  $^{18}\text{F}$  imply that it is consistent with zero, whereas the analysis of the  $^{133}\text{Cs}$  anapole moment yields a value for  $h_\pi^1$  that differs from zero by several standard deviations (7). More to the point, the connection between the PV experiments and SM expectations is far from transparent. Drawing this connection using the meson-exchange framework and nuclear PV observables requires sorting through a number of model-dependent effects involving nuclear structure, hadron structure, and the meson-exchange model itself. Whether this is possible to do in a systematic manner is debatable at best.

Ultimately the goal of studying the  $\Delta S = 0$  HWI with hadronic and nuclear PV is to help determine the degree to which the symmetries of QCD characterize the realization of the HWI in strongly interacting systems and, as a corollary, to shed light on the long-standing puzzles in the  $\Delta S = 1$  sector. To make contact with the underlying SM, the problem would ideally be formulated as transparently as possible and would avoid hadronic model and nuclear structure ambiguities. Recently, a framework for doing so was formulated by Zhu et al. (8) using EFT ideas. That work builds on the extensive developments in the past decade of an EFT for the strong NN interaction that has been applied successfully to a variety of few-body nuclear phenomena. In the case of the PV NN force, two versions of

---

<sup>1</sup>In the literature, the isovector PV  $\pi$ NN coupling is often denoted  $f_\pi$ . Here, however, we adopt the  $h_\pi^1$  notation to avoid confusion with the pion decay constant.

the EFT are useful, depending on the energy scales present in the process under consideration:

1. For energies well below the pion mass, the EFT contains only four-nucleon operators and five effective parameters, or low-energy constants (LECs), that characterize the five independent low-energy S-wave/P-wave mixing matrix elements:  $\lambda_s^{0,1,2}$ ,  $\lambda_t$ , and  $\rho_t$ . Relative to the leading order (LO) parity-conserving four-nucleon operators, the PV operators are  $\mathcal{O}(Q)$ , where  $Q$  is a small energy scale. In this version of the EFT, the pion is considered heavy and does not appear as an explicit, dynamical degree of freedom.
2. At higher energies, the pion becomes dynamical and two additional constants associated with  $\pi$ -exchange effects appear at lowest order:  $h_\pi^1$  and a new meson-exchange current operator characterized by  $\bar{C}_\pi$ . Moreover, the EFT incorporates the effects of two-pion exchange in a systematic way for the first time, leading to predictions for a medium-range component of the PV NN interaction (see Note Added in Proof).

The essential differences between the PV EFT and the meson-exchange frameworks—as well as their similarities—are summarized in Figure 1.

Clearly, implementing the EFT approach to the  $\Delta S = 0$  HWI requires carrying out new experiments in few-body systems in which ab initio structure computations can be performed. As outlined by Zhu et al. (8), a program of such measurements exists in principle. From a practical standpoint, carrying it out will involve meeting a number of experimental challenges. In light of new theoretical developments and experimental opportunities, we believe it is time to review the field of hadronic PV anew. Comprehensive reviews of the subject have appeared over the years, including the influential *Annual Review of Nuclear and Particle Science* review by Adelberger & Haxton (9) completed two decades ago. We hope to provide the successor to that work, updating the authors' analysis in light of new theoretical and experimental progress. Because our focus is on new developments, we touch only lightly on older work that has been reviewed by Adelberger & Haxton and elsewhere (9–11). Before doing so in detail, however, it is useful to summarize the primary developments and shifts in emphasis that have occurred since Adelberger & Haxton's review appeared:

1. The extensive development of  $\chi$ PT and NN EFT, together with substantial progress in performing lattice QCD simulations, has revolutionized our approach to treating hadronic physics. Although the use of hadronic models can provide important physical insights, the present day “holy grail” is to derive first-principles QCD predictions for hadronic phenomena. At the time of the Adelberger & Haxton review, the quark model was still in vogue, whereas the potential of lattice QCD and hadronic EFTs had yet to be realized. Today the situation is reversed. Indeed, in the case of  $\Delta S = 0$  HWI, the use of a meson-exchange model for the NN interaction that entails a truncation of

the QCD spectrum and contains effective couplings that likely parameterize more physics than the elementary meson-nucleon PV interaction (e.g., two- $\pi$ -exchange, TPE) obscures rather than clarifies the connection with the SM. We now know how to do better.

2. New experimental and technological developments have opened the way to performing PV experiments in few-body systems. The landscape now differs substantially from that of the 1980s, at which time it appeared that measuring a number of  $\mathcal{O}(10^{-7})$  effects in few-body processes was impractical. Indeed, two decades ago, the presence of the nuclear enhancement factors made experiments in many-body nuclei such as  $^{18}\text{F}$  more attractive than those in few-body systems. Since then, precise new measurements of  $10^{-7}$  PV observables in  $\vec{p}p$  scattering,  $\vec{n}\alpha$  spin rotation, and polarized neutron capture on hydrogen have either been completed or are in progress, and plans are being developed for other similarly precise few-body measurements at NIST, LANSCE, the SNS, and IASA (Athens). As we discuss below, completion of a comprehensive program of few-body measurements is now a realistic prospect.
3. Enormous progress has been made in performing precise, ab initio calculations in the few-body system using Green's function and variational Monte Carlo methods. These computations start with state-of-the-art phenomenological potentials that incorporate our present knowledge of NN phase shifts and include minimal three-body forces as needed to reproduce the triton binding energy and other three-body effects. A marriage between the NN EFT methods and these few-body computational approaches is also being developed. As a result, performing precise computations with the PV EFT for few-body observables is a realistic prospect, eliminating the nuclear structure questions that complicate the interpretation of many-body PV observables.

In short, the frontier today for understanding the  $\Delta S = 0$  HWI lies in the few-body arena, for which a combination of precise experiments and first-principles theory provides new tools for making the most direct possible confrontation with the interplay of the strong and electroweak sectors of the SM. The remainder of this review elaborates on this approach.

## 2. WEAK MESON-EXCHANGE MODEL MEETS THE END OF THE ROAD

Although the era of the meson-exchange framework for hadronic PV is drawing to a close, it has played such a central role in the field that its development and use following the publication of Reference 9 calls for a brief review. The primary theoretical developments have included updated theoretical “reasonable ranges” and “best values” for the  $h_M^i$  provided by DDH and others (6, 12, 13), analysis of

nuclear anapole moments extracted from atomic PV experiments, computations of nuclear PV contributions to PV electron scattering asymmetries, and new global fits of the  $h_M^i$  to nuclear and hadronic PV data. Experimentally, there has been the completion of the TRIUMF 221 MeV  $\vec{p}\vec{p}$ -scattering experiment, a neutron spin rotation experiment at NIST, the launching of an  $n\vec{p} \rightarrow d\gamma$  experiment at LANCSE, and the first nonzero result for a nuclear anapole moment in an atomic PV experiment with  $^{133}\text{Cs}$ .

## 2.1. Meson-Exchange Model of the Weak Nucleon-Nucleon Interaction

The meson-exchange, PV NN potential,  $V_{\text{DDH}}^{\text{PV}}$ , is generated by the meson-exchange diagrams of Figure 1a, wherein one meson-nucleon vertex is parity conserving and the other is parity violating. The Lagrangians for each set of interactions are widely available in the literature, so we give only the final form of the static potential:

$$\begin{aligned}
V_{\text{DDH}}^{\text{PV}}(\vec{r}) = & i \frac{h_\pi^1 g_A m_N}{\sqrt{2} F_\pi} \left( \frac{\vec{\tau}_1 \times \vec{\tau}_2}{2} \right)_3 (\vec{\sigma}_1 + \vec{\sigma}_2) \cdot \left[ \frac{\vec{p}_1 - \vec{p}_2}{2m_N}, w_\pi(r) \right] \\
& - g_\rho \left( h_\rho^0 \vec{\tau}_1 \cdot \vec{\tau}_2 + h_\rho^1 \left( \frac{\vec{\tau}_1 + \vec{\tau}_2}{2} \right)_3 + h_\rho^2 \frac{(3\tau_1^3 \tau_2^3 - \tau_1 \cdot \tau_2)}{2\sqrt{6}} \right) \\
& \times \left( (\vec{\sigma}_1 - \vec{\sigma}_2) \cdot \left\{ \frac{\vec{p}_1 - \vec{p}_2}{2m_N}, w_\rho(r) \right\} \right) \\
& + i(1 + \chi_\rho) \vec{\sigma}_1 \times \vec{\sigma}_2 \cdot \left[ \frac{\vec{p}_1 - \vec{p}_2}{2m_N}, w_\rho(r) \right] \\
& - g_\omega \left( h_\omega^0 + h_\omega^1 \left( \frac{\vec{\tau}_1 + \vec{\tau}_2}{2} \right)_3 \right) \\
& \times \left( (\vec{\sigma}_1 - \vec{\sigma}_2) \cdot \left\{ \frac{\vec{p}_1 - \vec{p}_2}{2m_N}, w_\omega(r) \right\} \right) \\
& + i(1 + \chi_\omega) \vec{\sigma}_1 \times \vec{\sigma}_2 \cdot \left[ \frac{\vec{p}_1 - \vec{p}_2}{2m_N}, w_\omega(r) \right] \\
& - \left( g_\omega h_\omega^1 - g_\rho h_\rho^1 \right) \left( \frac{\vec{\tau}_1 - \vec{\tau}_2}{2} \right)_3 (\vec{\sigma}_1 + \vec{\sigma}_2) \cdot \left\{ \frac{\vec{p}_1 - \vec{p}_2}{2m_N}, w_\rho(r) \right\} \\
& - g_\rho h_\rho^1 i \left( \frac{\vec{\tau}_1 \times \vec{\tau}_2}{2} \right)_3 (\vec{\sigma}_1 + \vec{\sigma}_2) \cdot \left[ \frac{\vec{p}_1 - \vec{p}_2}{2m_N}, w_\rho(r) \right]. \tag{2}
\end{aligned}$$

Here  $\vec{p}_i = -i\vec{\nabla}_i$ , with  $\vec{\nabla}_i$  denoting the gradient with respect to the coordinate  $\vec{x}_i$  of the  $i$ -th nucleon,  $r = |\vec{x}_1 - \vec{x}_2|$  is the separation between the two nucleons,

$$w_i(r) = \frac{\exp(-m_i r)}{4\pi r} \tag{3}$$

**TABLE 1** Theoretical reasonable ranges (column two) and best values (columns 3–5) for the PV meson-nucleon couplings (45)  $h_M^i$ , from DDH (6), Dubovic & Zenkin (DZ) (12), and Feldman et al. (FCDH) (13)

PV coupling	DDH range	DDH best value	DZ	FCDH
$h_\pi^1$	0 → 30	+12	+3	+7
$h_\rho^0$	30 → -81	-30	-22	-10
$h_\rho^1$	-1 → 0	-0.5	+1	-1
$h_\rho^2$	-20 → -29	-25	-18	-18
$h_\omega^0$	15 → -27	-5	-10	-13
$h_\omega^1$	-5 → -2	-3	-6	-6

All values are quoted in units of  $g_\pi = 3.8 \times 10^{-8}$ .

is the standard Yukawa function, and the strong  $\pi$ NN coupling  $g_{\pi NN}$  has been expressed in terms of the axial-current coupling  $g_A$  using the Goldberger-Treiman relation  $g_{\pi NN} = g_A m_N / F_\pi$ , with  $F_\pi = 92.4$  MeV as the pion decay constant. The  $g_V$ ,  $V = \rho, \omega$ , are the strong vector meson-nucleon Dirac couplings, and the  $\chi_V$  give the ratio of the strong Pauli and Dirac couplings. The terms in Equation 2 display different dependences on isospin and spin, so that various observables are sensitive to distinct linear combinations of the weak meson-nucleon couplings  $h_M^i$ . A notable feature is the absence of a neutral  $\pi$ -exchange component. Indeed, the only manifestation of  $\pi$ -exchange appears in the first term of Equation 2, which contains only products of the isospin raising and lowering operators for the two nucleons. This feature reflects a more general theorem by Barton (14) that forbids a neutral pseudoscalar-exchange component in the PV potential when CP is conserved.

The values of the  $h_M^i$  appearing in  $V_{DDH}^{PV}$  are most conveniently expressed in units of  $g_\pi$ , the natural strength for the weak  $\Delta S = 1$   $B \rightarrow B'\pi$  couplings:<sup>2</sup>

$$g_\pi = 3.8 \times 10^{-8} \approx \frac{G_F F_\pi^2}{2\sqrt{2}}. \quad 4.$$

The original DDH reasonable ranges and updated best values are given in Table 1. Note that no prediction for  $h_\rho^1$  appears, as DDH were unable to compute this constant in Reference 6. Subsequently, Holstein (15) used a  $1/2^-$  pole model to estimate this parameter. Using the quark model to compute the  $1/2^- \leftrightarrow 1/2^+$  mixing matrix elements, he obtained  $h_\rho^1 \simeq 1.8 g_\pi$ . Henceforth, we do not refer to this prediction when referring to the DDH values.

The various  $SU(6)_w$  symmetry arguments, current algebra techniques, and quark model estimates that lead to the values in Table 1 have been discussed in detail elsewhere (6, 13), and because our emphasis lies on a new formulation in which

<sup>2</sup>Here  $B$  and  $B'$  denote octet baryons.

these couplings do not appear, we do not revisit those discussions here. Instead, we concentrate on new applications of this framework.

**2.1.1. ANAPOLE EFFECTS** Two particularly novel uses of the PV meson-exchange framework have been in the analysis of atomic PV experiments and PV electron scattering. Shortly after PV was observed in  $\mu$ -decay and  $\beta$ -decay, Zeldovich & Vaks (16) pointed out that weak interactions could also induce a PV coupling of the photon and fermion. EM gauge invariance implies that the lowest-dimension effective operator for this coupling has the form (17)

$$\mathcal{L}_{\text{PV}}^{ff\gamma} = \frac{F_A}{\Lambda^2} \bar{\psi}_f \gamma_\mu \gamma_5 \psi_f \partial_\nu F^{\mu\nu}, \quad 5.$$

where  $F^{\mu\nu}$  is the EM field strength tensor,  $F_A$  is the anapole coupling, and  $\Lambda$  is an appropriate mass scale. This effective operator leads to the momentum-space interaction

$$M_{\text{PV}}^{eff} = -\frac{F_A}{\Lambda^2} \bar{u}(p)[q^2 \gamma_\mu - \not{q} q_\mu] \gamma_5 u(p) \varepsilon^\mu(q), \quad 6.$$

where  $q = p' - p$  is the momentum of a photon with polarization vector  $\varepsilon^\mu(q)$ . From Equation 6 it is clear that the anapole coupling involves only virtual photons because for a real photon,  $q^2 = 0$  and a gauge in which  $q \cdot \varepsilon = 0$  can always be chosen. Because  $\partial_\nu F^{\mu\nu} = J^\mu$ , Equation 5 implies that the anapole interaction effectively couples the fermion axial current to the source of the EM field  $J^\mu$ .

In the 1980s, Flambaum and colleagues (18, 19) observed that the anapole moments of nuclei should scale as the square of the nuclear radius, rather than as  $1/\Lambda^2$ , so that their magnitudes would be enhanced as  $A^{2/3}$  in heavy nuclei. Moreover, the nuclear anapole moment couples the nuclear axial current to the EM currents of the atomic electrons, thereby inducing a PV, nuclear spin-dependent term in the atomic Hamiltonian. Experimentally, observing nuclear spin-dependent transitions in atomic PV processes could isolate this effect. As we discuss below, a nonzero result for the  $^{133}\text{Cs}$  anapole moment has been obtained by the Boulder group, whereas the Seattle group has placed limits on the anapole moment of  $^{205}\text{Tl}$ . Efforts are presently underway to measure the anapole moments of other nuclei, such as Fr (for recent reviews, see e.g., References 20, 21, and 22).

The new anapole moment measurements have stimulated considerable theoretical activity. Using a one-body averaged version of  $V_{\text{DDH}}^{\text{PV}}$  and a simple single particle shell model, Flambaum and colleagues (18, 19) estimated the magnitudes of the anapole moments of various nuclei, demonstrating the  $A^{2/3}$  scaling under these conditions. Substantially more sophisticated shell model calculations using the complete two-body potential and associated meson-exchange currents were carried out in References 7, 23 and 24. The results have been used to extract constraints on the DDH couplings, as shown in Figure 2. Of particular interest is the significant disagreement between the  $^{133}\text{Cs}$  anapole constraints on the relevant isovector combination of couplings, compared with those obtained from the

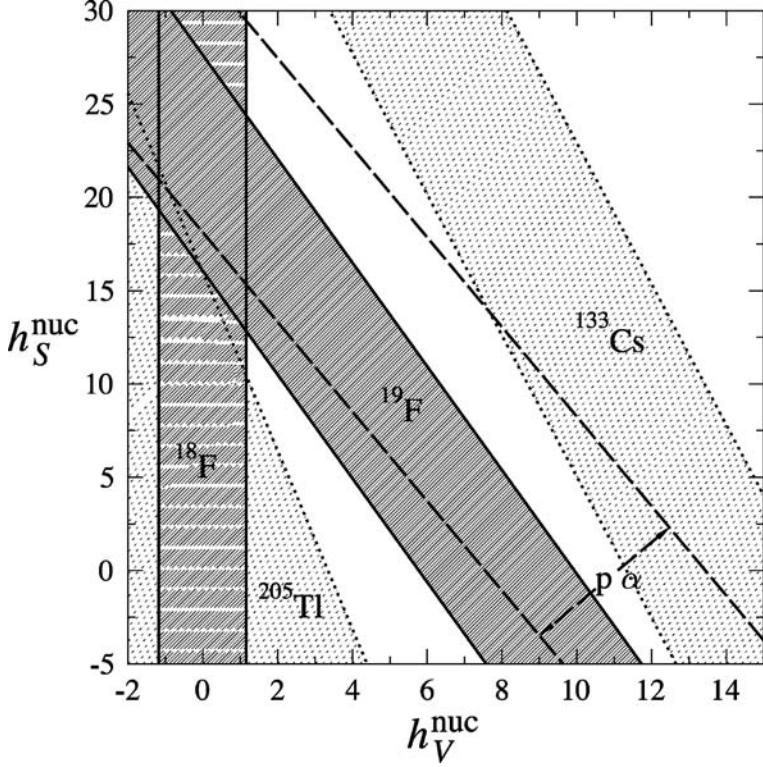


**Figure 2** Constraints on effective DDH weak meson-nucleon couplings deduced from parity-violating observables in nuclei and anapole moments of heavy atoms. Here,  $h_V^{\text{nuc}} = h_\pi^1 - 0.12h_\rho^1 - 0.18h_\omega^1$  and  $h_S^{\text{nuc}} = -(h_\rho^0 + 0.7h_\omega^0)$ . (Figure courtesy of W.C. Haxton.)

circular polarization  $P_\gamma$  in the  $\gamma$ -decay of  $^{18}\text{F}$ . Other nuclear model computations of the  $^{133}\text{Cs}$  anapole moment, having greater or lesser degrees of sophistication, lead to similar conclusions (25–30).

As discussed in References 7 and 24 state-of-the-art shell model computations unavoidably entail model-space truncations, and in the case of the Cs anapole moment calculations, inclusion of the omitted contributions would likely increase, rather than decrease, the disagreement with the  $^{18}\text{F}$  result. In contrast, the nuclear structure analysis used to interpret the  $P_\gamma$  results appears robust because the dominant nuclear mixing matrix element can be calibrated against an analog  $\beta$ -decay amplitude (31, 32). Thus, the implications of the new result for the Cs anapole moment are quite puzzling.

The  $\Delta S=0$  HWI can also contribute to the PV asymmetry  $A_{PV}$  measured in the scattering of longitudinally polarized electrons from hadronic and nuclear

targets. In the late 1990s, physicists realized that the anapole moment of the proton contributes to  $A_{\text{PV}}$  for elastic  $\vec{e}p$  scattering in a way that is indistinguishable from that of the axial vector coupling of the  $Z^0$  to the proton, or  $G_A^e$  (Figure 3) (33). Moreover, theoretical analysis showed—using the DDH framework—that both the magnitude of the proton anapole moment contribution as well as the theoretical uncertainty associated with it was sufficiently large as to significantly affect the interpretation of  $A_{\text{PV}}$ . At that time, a program of PV electron scattering measurements was being developed to determine the strange quark contributions to the electric and magnetic form factors of the proton,  $G_E^s$  and  $G_M^s$ , respectively. The presence of the anapole-related uncertainties would be particularly problematic for the extraction of  $G_M^s$  from the backward-angle asymmetry measurements (34, 35).

Consequently, additional measurements of  $A_{\text{PV}}$  for quasi-elastic (QE) scattering from the deuteron were carried out. Because the deuteron asymmetry is strongly sensitive to  $G_A^e$  but considerably less sensitive to  $G_M^s$  than is the proton asymmetry, a measurement of  $A_{\text{PV}}^{\text{QE}}(\vec{e}D)$ —in conjunction with  $A_{\text{PV}}^{\text{El}}(\vec{e}p)$ —can be used to test the theoretical estimates of Reference 33, while providing for a determination of  $G_M^s$  that is independent of hadronic PV uncertainties. The initial results of these measurements, completed by the SAMPLE collaboration (36), yielded a new puzzle: The effective  $G_A^e$  extracted from the  $\vec{e}p$  and  $\vec{e}D$  asymmetries was consistent with zero. The calculations of Reference 33 had predicted a  $\sim 40\%$  reduction to the value of  $G_A^e$  arising from SM electroweak radiative corrections and the anapole effect. The SAMPLE result, however, implied a substantial enhancement of the anapole contribution or that of other radiative corrections over the predictions of Reference 33.

Subsequent theoretical studies attempted to determine the origin of the anomaly, scrutinizing various contributions to  $A_{\text{PV}}$ : The original computation of Reference 33 was revisited and updated using heavy baryon  $\chi$ PT (37), possible quark model enhancements were considered (38), the  $q^2$  dependence of the anapole contribution was studied (39, 40), and contributions from parity mixing in the deuteron and final  $np$  states were computed using the meson-exchange model (41, 42). No large effects that could resolve the puzzle were found in any of these studies. Ultimately, the SAMPLE collaboration carried out a reanalysis of the pion-production background in the deuteron experiment that shifted the value of  $A_{\text{PV}}^{\text{QE}}(\vec{e}D)$  (43) and brought the axial term into agreement with the predictions of References 33 and 37. The theoretical results from the latter work have now been used in extracting  $G_M^s$  from the backward-angle proton asymmetry (44).

Within the DDH framework, these developments—in addition to the completion of a new  $\vec{p}\vec{p}$ -scattering experiment at TRIUMF—have motivated reanalyses of the hadronic and nuclear PV observables in terms of the  $h_M^i$ . After discussing the recent experimental developments, we summarize our current understanding of hadronic PV in this context and make the case that a fundamental paradigm shift is required to progress further in this field.

## 2.2. Experimental Progress

Earlier reviews, e.g., References 9, 45, and 46, have documented an extensive body of experimental work aimed at characterizing the  $\Delta S = 0$  HWI, largely carried out in many-body nuclei. As noted in the Introduction, the PV effects in the much simpler NN and few-nucleon systems were almost impractically small [ $\mathcal{O}(10^{-7})$ ] from the standpoint of past experimental feasibility, so the realization of fortuitous nuclear structure effects that amplify the underlying NN PV signal by several orders of magnitude naturally led to an earlier focus on many-body systems. Future progress hinges on a handful of precise experiments in much simpler few-nucleon systems, for which the theoretical interpretation is less fraught with model-dependent uncertainties and for which precise measurements now appear to be realistic. Here, we review recent experimental progress in the few-body sector and comment on new developments in probes of PV in many-body nuclei. These developments have been cast largely in the weak meson-exchange framework, so we discuss their theoretical implications here. When developing the EFT framework in Section 3, we reframe the discussion of these theoretical implications in the EFT formulation.

Probing the NN weak interaction in few-body systems presents significant experimental challenges. The bare NN  $\mathcal{O}(10^{-7})$  PV effects compete with a host of potential systematic errors at this level, which must be both minimized through careful experimental design and simultaneously measured to ensure that they do not obscure the true PV signal. Even acquiring sufficient data to reach a statistical error at the  $10^{-7}$ – $10^{-8}$  level is no mean feat, necessitating the use of current-mode detection, which in turn introduces its own systematic error sensitivities that must be controlled and understood. The most accessible NN and few-nucleon observables are accessed in polarized beam experiments, in which rapid polarization reversal provides a practical means of suppressing low-frequency noise and systematic effects at the expense of introducing a built-in sensitivity to spin-correlated beam properties that can mimic the PV observable in question. In such cases, as much effort must be expended to optimize and characterize the polarized beam properties as is required to design and commission the PV experimental apparatus. Typically, a successful experiment spans a decade or more from initial conception to publication of a significant result, with continuous refinements of the experimental apparatus and technique until the desired sensitivity is reached. Typically, an order of magnitude more data are required to refine and test the apparatus than to acquire the final PV data sample.

To date, there have been a number of significant measurements of PV in  $\vec{p}p$  scattering, but despite several decades of experimental effort, a definitive observation of PV in the  $np$  system remains to be established. Recent experimental progress in the NN system includes the completion of a program of high-precision measurements of PV in  $\vec{p}p$  scattering, which yield independent constraints on the weak couplings of heavier mesons, and the commissioning of a PV asymmetry measurement in  $\vec{n}p \rightarrow d\gamma$  that is aimed at a precise determination of  $h_{\pi}^1$ . These

experiments are discussed briefly below; future possibilities for precise measurements in two- and few-nucleon systems are discussed in Section 3.

**2.2.1. LONGITUDINAL ANALYZING POWER IN  $\vec{p}\vec{p}$  SCATTERING** The PV observable studied in  $\vec{p}\vec{p}$  scattering is the longitudinal analyzing power  $A_z = \frac{(\sigma^+ - \sigma^-)}{(\sigma^+ + \sigma^-)}$ , where  $\sigma^+$  and  $\sigma^-$  are the elastic scattering cross sections for positive and negative helicity beams incident on an unpolarized hydrogen target. The analyzing power can be naturally expressed as a sum of parity-mixed partial wave contributions, with only S-P mixing required to characterize  $A_z$  at low energy. The first two partial waves in the expansion are sufficient to describe  $A_z$  up to several hundred MeV; the ( $^1S_0 - ^3P_0$ ) contribution dominates at low energy, whereas the ( $^3P_2 - ^1D_2$ ) amplitude becomes significant above 100 MeV. These two partial wave amplitudes have complementary dependences on the weak meson-nucleon couplings:  $h_\rho^{pp} = (h_\rho^0 + h_\rho^1 + h_\rho^2/\sqrt{6})$  and  $h_\omega^{pp} = h_\omega^0 + h_\omega^1$ . As noted by Simonius (47), the dominant S-P wave mixing integrates to zero near 220 MeV beam energy owing to a fortuitous cancellation of the strong S- and P-wave phase shifts. This observation motivated the recently completed TRIUMF experiment at 221 MeV (48), which was designed to isolate ( $^3P_2 - ^1D_2$ ) contribution.

Although earlier high-precision measurements at low energy were performed in a total scattering geometry, the TRIUMF 221 MeV measurements were carried out in transmission mode. The small size of the total scattering asymmetry  $A_z \simeq 10^{-7}$  implied a transmission asymmetry of order  $10^{-9}$  for the TRIUMF experiment. Integrating detectors with small angular acceptance coupled to low-noise electronics, excellent beam and liquid hydrogen target stability, and a highly polarized beam with minimal helicity-correlated beam properties were essential to the success of the measurements. Rapid beam polarization reversal (40 Hz, with controlled phase slip with respect to the line frequency) led to an ac PV signal at a well-determined frequency, greatly suppressing the noise contributions with respect to a dc measurement (which would be impossible in this case owing to the extremely small size of the PV asymmetry signal). The principle of the TRIUMF transmission-mode measurement is illustrated in Figure 4.

The TRIUMF Laboratory spent many years developing a state-of-the-art optically pumped polarized  $H^-$  ion source (49, 50), which was ideal for demanding symmetry tests that require polarized beam, as the polarization ( $\simeq 85\%$ ) was reversed by changing the frequency of the laser light without changing macroscopic electric or magnetic fields that could influence the beam properties. Even so, significant corrections ( $\simeq 40\%$ ) had to be made to the raw asymmetry for helicity-correlated transverse polarization components.

Transverse polarization is a pathological source of systematic error in  $\vec{p}\vec{p}$ -scattering measurements because of the relatively enormous parity-allowed transverse analyzing power  $A_y$ , which is more than one million times larger than the PV longitudinal analyzing power  $A_z$ . Although it is not practical to demonstrate and maintain tiny transverse polarization components at or below the  $10^{-6}$  level,

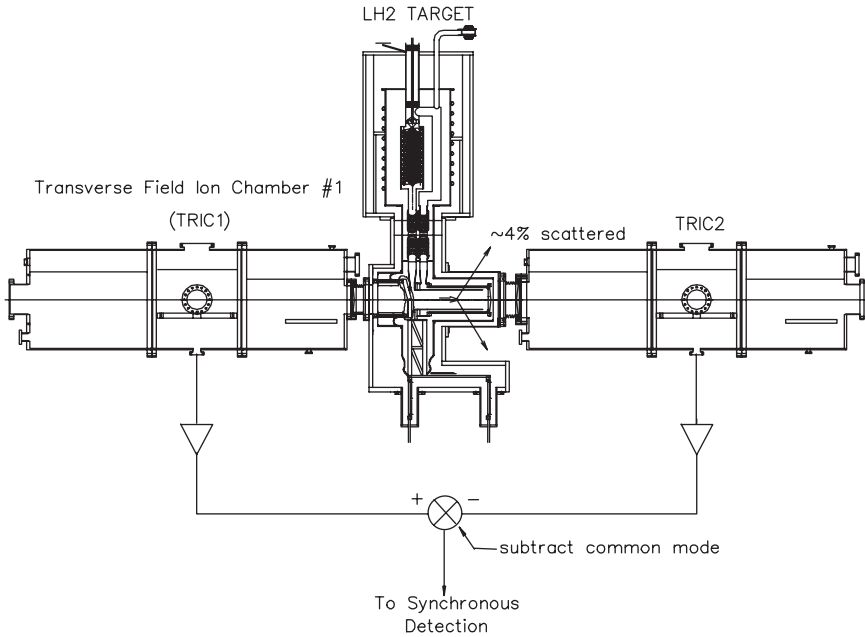


**Figure 4** Principle of the TRIUMF  $p\bar{p}$  parity violation experiment. Longitudinally polarized protons at 221 MeV passed through a 40-cm liquid hydrogen target (LH2), which scattered  $\simeq 4\%$  of the beam. The polarization-dependent target transmission was measured by performing an analog subtraction of two dc current signals from transverse field ionization chambers. [Reprinted with permission from Reference 48, Figure 1. Copyright by the American Physical Society (2003).]

fortunately the geometrical symmetry of the apparatus can be invoked to establish a neutral axis for the beam transport such that the false asymmetry arising from transverse polarization components is identically zero if the beam is locked on this axis by a position feedback system. This technique ensured that corrections for average transverse polarization components  $\langle P_y \rangle$  and  $\langle P_x \rangle$  were insignificant at the  $10^{-9}$  level in the TRIUMF measurements—the associated corrections  $\Delta A_z$ , e.g., for transverse vertical polarization  $\langle P_y \rangle$ , scale as  $\langle x \rangle \langle P_y \rangle$ , where  $\langle x \rangle$  is the net displacement from the symmetry axis whose location can be determined by separate calibration experiments. The form of the driving term  $\langle x \rangle \langle P_y \rangle$  is that of the first moment of transverse polarization at the detector location, which is referred to as an extrinsic first moment; a similar correction must also be made for intrinsic first moments of the form  $\langle x P_y \rangle$ , which arise from nonuniform distributions of transverse polarization within the beam envelope. These extrinsic polarization moments are extremely difficult to measure and control.

The TRIUMF experiment employed a pair of scanning polarimeters (51) to provide continuous measurements of the distribution of transverse polarization

components within the beam, interleaved with parity data taking from the transverse ion chambers on an 8-state, 200-ms data cycle. The limiting factor in the TRIUMF experiment was the statistical precision of the polarization profile monitors (PPMs), which were coincidence counting-mode devices. An essential assumption made in determining the correction for intrinsic polarization moments was that the moments evolved linearly with position along the beamline and thus had a stable ratio between upstream and downstream PPMs. This ratio could in principle be tuned to achieve a null sensitivity to intrinsic polarization moments, an approach modeled on the successful polarization neutral axis idea described above. Unfortunately, the ability of the PPMs to measure this first-moment ratio sufficiently and precisely in a reasonable amount of time was severely limited and so significant corrections still had to be made to the data.

Research and development efforts toward a follow-up experiment at higher energy (which was never realized) included development of a current-mode scanning polarimeter that had  $\sim 20$  times greater statistical precision (52); the current-mode polarimeter clearly demonstrated the constant linear evolution of intrinsic moments along the beamline, as illustrated in Figure 5, thus independently validating the corrections procedure used to obtain a final result for  $A_z$  at 221 MeV from TRIUMF experiment 497.

Parity violation in  $\vec{p}\vec{p}$  scattering has attracted considerable theoretical interest since Adelberger & Haxton's review (9). Recent calculations are shown in Figure 6, together with the most precise experimental data at low and intermediate energies. Driscoll & Miller (53, 54) used the Bonn potential to treat the strong NN interaction, with weak meson-nucleon couplings taken from Reference 6. Iqbal & Niskanen's (55) calculation adds a  $\Delta$  isobar contribution to the Driscoll & Miller model. The calculation of Driscoll & Meissner (56) is based on a chiral soliton model, whereas the quark model calculation of Grach & Shmatikov (57) takes explicit account of quark degrees of freedom.

Figure 7 by Carlson et al. (58) shows the limits on the weak meson-nucleon couplings  $h_\rho^{pp}$  and  $h_\omega^{pp}$  imposed by the low-energy  $\vec{p}\vec{p}$  asymmetry measurements and the 221 MeV TRIUMF result. The error bands are based on a calculation assuming the Argonne  $v_{18}$  (AV-18) potential (59) and the Bonn 2000 (CD-Bonn) (60) strong interaction coupling constants, and including all partial waves up to  $J = 8$ . Although the TRIUMF measurement is not sensitive to  $A_z$  from S-P mixing, and the contribution from P-D mixing contains no  $h_\omega^{pp}$  contribution, there is some  $h_\omega^{pp}$  dependence arising from higher partial waves. The best fit to the  $\vec{p}\vec{p}$  data yields  $h_\rho^{pp} = -22.3 \times 10^{-7}$  and  $h_\omega^{pp} = 5.17 \times 10^{-7}$ , compared with the DDH "best guess" values of  $h_\rho^{pp} = -15.5 \times 10^{-7}$  and  $h_\omega^{pp} = -3.0 \times 10^{-7}$ .

**2.2.2. PROGRESS IN THE  $np$  SYSTEM** Parity violation in the  $np$  system can in principle be detected in a variety of processes that can reveal complementary aspects of the weak NN interaction. In  $np$  capture, there are two complementary PV observables:  $P_\gamma^d$ , the 2.2 MeV  $\gamma$ -ray circular polarization for an unpolarized neutron beam, and  $A_\gamma^d$ , the asymmetry in the emission of  $\gamma$ -rays with respect to the

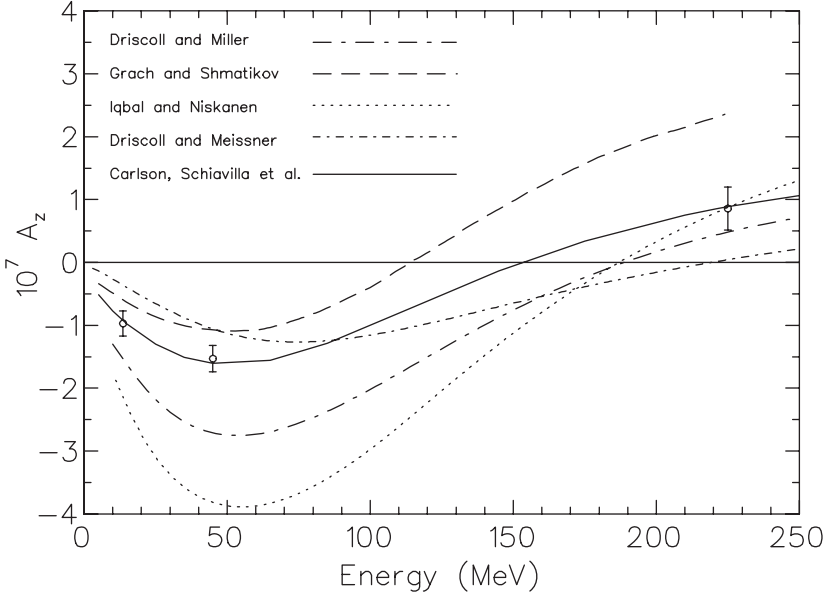


**Figure 6** The most precise measurements of parity violation in  $pp$  scattering at low and intermediate energy, and recent theoretical predictions. Experiments were performed at Bonn (13.6 MeV) (143), PSI (45 MeV) (144), and TRIUMF (221 MeV) (48). The solid curve shows the calculation by Carlson et al. (58), including a fit of the weak meson-nucleon coupling constants to the data. [Reprinted with permission from Reference 48, Figure 13. Copyright by the American Physical Society (2003).]

neutron spin direction if the beam is polarized. Closely related to the first of these,  $P_\gamma^d$ , is the helicity asymmetry  $A_L^\gamma$  in the photodisintegration of deuterium with circularly polarized photons; the two are asymptotically equal to each other at threshold, whereas  $A_L^\gamma$  is predicted to drop rapidly with increasing photon energy, falling an order of magnitude as the photon energy increases to 1 MeV above threshold (61). Finally, the transmission of polarized neutrons through hydrogen should reveal a tiny PV spin rotation about the neutron propagation direction  $\hat{z}$ :  $d\phi^{np}/dz$ .

Unfortunately, all of these  $np$  system measurements are extremely challenging; the first three have been attempted (62–64) but have yielded null results with limits at least one order of magnitude too large to provide a meaningful constraint on the weak meson-exchange predictions (61, 65–68), all of which are at the level  $5 \times 10^{-8}$  or smaller. The two PV observables involving the  $np$  capture reaction,  $P_\gamma^d$  and  $A_\gamma^d$ , have complementary dependences on the weak meson-nucleon couplings—notably,  $A_\gamma^d$  can yield a unique constraint on  $h_\pi^1$ , whereas  $P_\gamma^d$  depends on a linear combination of  $\pi$ ,  $\rho$ , and  $\omega$  weak couplings (9). Measurement of  $\gamma$ -ray circular polarization requires a Compton polarimeter with typical sensitivity at the

few percent level, thus rendering the  $P_\gamma^d$  measurement in principle even more challenging than a measurement of  $A_\gamma^d$ . A measurement of the helicity asymmetry  $A_L^\gamma$  in the photodisintegration of deuterium is at the early conceptual design stage for the future experimental program at IASA (Athens) (69), with the aim of reaching a sensitivity at the  $10^{-8}$  level. The  $\vec{n}p$  spin rotation measurement, with an anticipated  $d\phi^{np}/dz = 5 \times 10^{-7}$  rad/m (70), has not yet been attempted but is envisioned as a future component of the SNS fundamental neutron physics program, as discussed in Section 3.4 below.

The intrinsic interest of a clean measurement of  $h_\pi^1$  in the NN system, together with considerations of experimental feasibility, has led to the launching of a major effort at LANSCE (71)—the NPDGamma experiment—to make a definitive measurement of  $A_\gamma^d$ , with an ultimate goal of reaching  $\pm 10\%$  of the DDH prediction. The measurement of  $A_\gamma^d$  requires a polarized neutron beam with precisely known spin direction and a measurement of the 2.22 MeV  $\gamma$ -ray angular distribution:  $\frac{d\omega}{d\theta} \sim (1 + A_\gamma \cos\theta)$ , where  $\theta$  is the angle between the  $\gamma$ -ray momentum and the neutron spin. Even at milli-eV neutron energies for neutrons moderated in liquid hydrogen, the scattering cross section exceeds the capture cross section by a significant factor. A parahydrogen target is essential to avoid neutron spin flip on scattering in the target, and the useful beam flux is below 15 meV to prevent depolarization in the target.

A previous measurement of  $A_\gamma^d$ , performed at the ILL reactor in the 1970s (64), reported a value of  $(0.6 \pm 2.1) \times 10^{-7}$ ; the NPDGamma experiment is designed to reach an ultimate sensitivity of  $\pm 5 \times 10^{-9}$ , with the uncertainty dominated by statistical rather than systematic errors. Major improvements in the experimental instrumentation and techniques that should make this possible include

1. use of a high-intensity, low-energy, pulsed beam, which allows for neutron energy determination via time-of-flight measurement and allows for a separation in time of prompt  $\gamma$ -ray background from the neutrons of interest;
2. polarization of the beam via selective transmission through optically pumped, polarized cells of  $^3\text{He}$ ; the well-known spin-dependent cross section leads to an energy-dependent polarization that can be very high for low-energy neutrons, and the beam polarization can be continuously and directly monitored by online measurements of the  $^3\text{He}$  cell transmission;
3. use of a resonant RF spin flipper capable of flipping spins at all neutron energies with high efficiency and eliminating Stern-Gerlach steering of the neutron beam associated with spin flip; and
4. implementation of a large solid-angle, high-efficiency CsI (TI) gamma detector array (72) instrumented with sensitive current-mode electronics whose intrinsic noise is negligible compared with neutron counting statistics.

Figure 8 shows a schematic of the NPDGamma apparatus mounted in the new experimental cave on Flight Path 12 at LANSCE. The neutron spins, polarized by the  $^3\text{He}$  transmission cell, are efficiently reversed by the RF spin flipper on

a pulse-by-pulse basis, thus alternating the sign of the PV asymmetry measured in the gamma detector array at 20 Hz. At the time of writing, NPDGamma has achieved a number of major milestones and is ready to take production data at LANSCE, pending installation of the liquid hydrogen target. The apparatus has been fully commissioned, electronic asymmetries are consistent with zero at the few  $\times 10^{-9}$  level, and PV asymmetries arising from neutron capture on a variety of solid targets, which are representative of materials used to construct the beamline and parity instrumentation, have been measured. All are consistent with zero at the  $10^{-6}$  level or smaller, with sufficient accuracy to conclude that background asymmetries will not play a significant role in the hydrogen target data. A known PV asymmetry in Cl at the  $10^{-5}$  level has been remeasured and will be used as a diagnostic tool for NPDGamma, with the periodic insertion of a  $\text{CCl}_4$  target to verify the consistent performance of the experimental setup. Contamination of the hydrogen target PV (up-down) asymmetry by the comparably small, parity-allowed left-right asymmetry will be kept below an acceptable level by determining the effective detector angles in situ—this in turn will be accomplished by scanning the detector array horizontally and vertically with respect to the target while acquiring  $np$  capture data. The measured Cl asymmetry is shown in Figure 9; the net PV (up-down) and parity-allowed left-right asymmetries deduced from these data (71) are  $A_\gamma = (-19 \pm 2) \times 10^{-6}$  and  $A_{LR} = (-1 \pm 2) \times 10^{-6}$ .

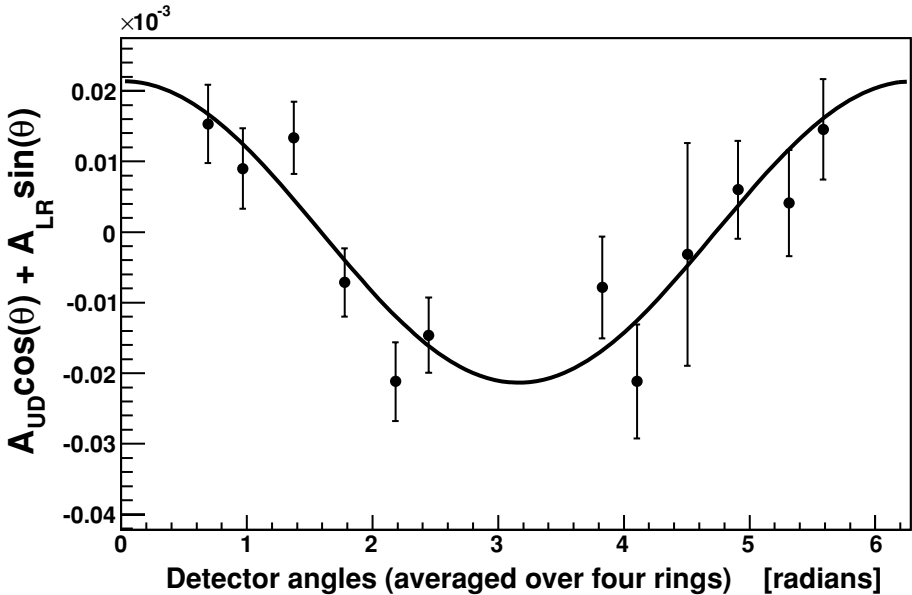


**Figure 9**  $\text{CCl}_4$   $\gamma$ -ray asymmetries for the NPDGamma 2004 data, calculated from opposing detector pairs, plotted versus the angle of the first detector in the pair with respect to the vertical. The total asymmetry  $A = A_\gamma \cos \theta + A_{LR} \sin \theta$  is deduced from the fit. (Figure courtesy of M.T. Gericke.)

Unfortunately, a number of factors have conspired to severely limit the statistical accuracy that can be achieved by running the NPDGamma experiment at LANSCE. These include a reduction by a factor of four of the available neutron flux per beam pulse as compared with expectations prior to the recent upgrade of the LANSCE facility and a further reduction in high-quality beam time due to magnetic interference from a neighboring experiment. In view of these limitations, the NPDGamma collaboration plans to carry out a first measurement with hydrogen in 2006, which would provide a statistics-limited result for  $A_\gamma^d$  accurate to  $\pm 1 \times 10^{-7}$  or better. At the time of writing, there are plans to move the experiment to the Fundamental Neutron Physics Beam (FNPB) at the SNS, which would enable the collaboration to make a measurement of  $A_\gamma^d$  to  $\pm 1 \times 10^{-8}$  or better, as discussed in Section 3.4.

**2.2.3. NEUTRON SPIN ROTATION EXPERIMENTS** Low-energy neutrons can exhibit a PV spin rotation induced by the HWI as they pass through a medium. The observable,  $\phi_{PV}$ , is the angle of transverse spin rotation about the neutron's direction of motion. In the limit of zero neutron energy, the PV neutron spin rotation is energy independent (73). After traversing a distance  $z$  through the medium, the neutron spin will precess by an amount  $\phi_{PV} = 2\pi\rho z f_{PV}$ , where  $f_{PV}$  is the PV coherent forward-scattering amplitude for a low-energy neutron and  $\rho$  is the number density of the medium (74). The basic requirements of a neutron spin rotation experiment are a source of low-energy polarized neutrons, a target containing the material of interest, and a spin analyzer downstream of the target, from which the value of  $\phi_{PV}$  can be deduced.

Two cases are particularly interesting from the standpoint of testing HWI models: PV neutron spin rotations in  $^1\text{H}$  and  $^4\text{He}$ . These two cases have complementary dependences on the weak meson-nucleon couplings  $h_M^i$ . The  $np$  case is dominated by the weak pion exchange contribution and thus yields similar information to the NPDGamma experiment described above. The  $^4\text{He}$  PV spin rotation has a significant contribution from  $h_\pi^1$  but is also sensitive to the  $h_\rho^0$  coupling. Experimentally, the  $^4\text{He}$  case is more tractable, owing to a much longer mean free path for low-energy neutrons than hydrogen. Like NPDGamma, the  $np$  spin rotation experiment requires a parahydrogen target to avoid neutron depolarization due to spin-exchange collisions with the hydrogen molecules, and only neutron energies below 15 meV would be useful for the experiment.

A  $^4\text{He}$  spin rotation measurement was carried out at NIST in the 1990s (75), with the result  $\phi_{PV} = (8 \pm 14_{stat} \pm 2_{sys}) \times 10^{-7}$  rad/m. Unfortunately this heroic effort did not reach sufficient sensitivity to test HWI models. Researchers have considered, but have not yet proposed, a possible experiment in hydrogen, and an experiment will hopefully be carried out at the SNS within the next decade (see Section 3.3).

What confounds the beautiful simplicity of the measurement principle is the extremely small size of the PV rotations expected on the basis of the DDH model: For  $^4\text{He}$ , the predicted effect is  $\phi_{PV} = -1 \times 10^{-7}$  rad/m (76), whereas for the proton, the effect should be approximately five times larger (70). These PV spin

rotations are eight orders of magnitude smaller than those induced by the Earth's magnetic field in a typical measurement apparatus! Therefore, a much more elaborate scheme is required to achieve the necessary sensitivity. Great care must be taken to reduce ambient magnetic fields by many orders of magnitude, residual fields must be monitored carefully, and the experiment should be designed so that in the extraction of the PV spin rotation angle, the effects of residual magnetic fields are cancelled to the maximum possible extent.

The basic experimental technique employed at NIST and foreseen for subsequent measurements involves a double beam/double cell apparatus, as shown in Figure 10. The double cell design incorporates a  $180^\circ$  spin precession about the initial spin direction between the two target cells, one of which is full and the other empty, for a given measurement. A clear advantage of the double cell design is that the much larger spin rotations due to residual magnetic fields cancel each other in the two target states to the extent that the magnetic fields and the neutron trajectories are exactly the same in both cases. An identical double target system sits beside the first one in the same cryostat; half the beam passes through each, and the two systems are run so that at any given time the signs of the PV spin rotation in the two subsystems are exactly opposite. Downstream of the double target system is a polarization analyzer and segmented  $^3\text{He}$  ionization chamber, which measures the counting rate in left and right elements of the apparatus simultaneously.

Instead of rapidly flipping the beam polarization as in the  $\vec{p}\vec{p}$  and NPDGamma experiments described above, the sign of the PV effect is reversed by alternating the location of the full target cell with respect to the  $\pi$  coil. The emptying and filling of the target cells took several minutes in the first spin rotation experiment, and each measuring interval was 10 min, corresponding to a reversal rate of 1 mHz and approximately 25% dead time. However, with a pair of double cell setups located side by side in the same cryostat, and a beam splitter upstream of the apparatus, reactor beam intensity fluctuations can be effectively cancelled, which makes up for the slow PV reversal frequency.

Features of the upgraded apparatus include improved magnetic shielding, resulting in a fourfold reduction of ambient fields to the  $20\ \mu\text{G}$  level; improved cryogenic systems with a faster target cycling time; operation with superfluid  $^4\text{He}$ , which has a much smaller total- and small-angle neutron scattering cross section than normal  $^4\text{He}$ ; and improvements to the NIST cold source, leading to a 50% increase in the beam fluence. These and other improvements should result in a statistical error of  $\pm 3 \times 10^{-7}$  rad/m in a three-month run at NIST during 2005–2006, with systematic errors (based on simulations of the experiment) at the  $10^{-8}$  level. Like NPDGamma, the collaboration proposes to move the  $^4\text{He}$  spin rotation experiment to the SNS, where the high-intensity pulsed cold neutron beam would permit a high-statistics measurement in approximately a year's running time, with greater diagnostic capability for systematic errors (137).

**2.2.4. NUCLEAR ANAPOLE MOMENTS** Nuclear anapole moments, which may be accessed via measurements of parity violation in atoms, have recently opened a new

window on the HWI (77). This subject has been the focus of significant theoretical and experimental efforts, including a recent review in this journal (20). A detailed discussion of experimental atomic physics approaches is beyond the scope of the present work; however, for completeness, we include a brief overview of experimental efforts here.

A prime motivation for atomic PV measurements is to provide stringent tests of the electroweak SM. The dominant contribution to the neutral weak electron-nucleus interaction arises from an axial coupling to the electron and a vector coupling to the nucleus and is proportional to the nuclear weak charge,  $Q_W$ . The value of  $Q_W$  can be computed with high accuracy in the SM, and a precise experimental determination of the nuclear weak charge can probe for deviations that are expected to arise from physics beyond the SM. This dominant PV contribution is nuclear spin independent, and the extraction of  $Q_W$  is minimally affected by HWI corrections. However, the weak electron-nucleus interaction also has a contribution from the vector coupling of the electron to the axial current of the nucleus; this leads to a nuclear spin-dependent PV interaction that can be detected as a small hyperfine dependence of atomic PV. The PV interaction in this case has contributions from  $Z^0$  exchange, a hyperfine interaction correction, and finally the nuclear anapole moment (7, 24).

The weak interaction typically induces very tiny opposite-parity wavefunction admixtures in atomic states, on the order of  $10^{-11}$ . These in turn give rise to extremely small and otherwise parity-forbidden transition amplitudes. The best explored case is atomic PV in Cs, measured in the highly forbidden  $6s-7s$  transition in an atomic beam in which the tiny PV amplitude was arranged to interfere with a much larger Stark-induced transition amplitude in the presence of a static E field.<sup>3</sup> The authors (77) report the use of 31 different servo systems to control precisely electrical, optical, and mechanical systems during the measurements; they designed an experiment with five independent means of reversing the parity signal and spent approximately 20 times more data-taking effort in the investigation and elimination of systematic errors compared with actual PV data taking. From the standpoint of atomic-structure calculations needed to interpret the measurements, the heavy alkali atom Cs is ideal for precision PV studies because of its relatively simple electronic configuration of one valence (6s) electron outside a tightly bound Xe noble gas core.

Because the nuclear anapole moment is expected to scale as  $A^{2/3}$  and the corresponding experimental signature scales as  $Z^2 A^{2/3}$ , heavy nuclei are the preferred systems for experimental studies. To date, a definitive experimental result exists only for the anapole moment of  $^{133}\text{Cs}$  (77), whereas an upper limit has been found for the anapole moment of Tl (30%  $^{203}\text{Tl}$ , 70%  $^{205}\text{Tl}$  isotopic ratio) (78) obtained via PV optical rotation measurements. In Cs, the nuclear spin-independent atomic PV effect has been measured to 0.4%, whereas the anapole moment contribution

<sup>3</sup>The advantage of this seemingly complicated experimental scheme is that, rather than trying to measure the forbidden transition rate, the interference technique yields an observable that is linear in the tiny PV amplitude.

has been determined to 14%. In Tl, the spin-independent effect has been measured to 3%, and the spin-dependent anapole contribution is consistent with zero. These are the results of truly heroic experimental investigations spanning more than a decade of instrumentation development and testing. Interpretation of the spin-independent PV as a SM test requires excellent understanding of the atomic structure, whereas the anapole moment must first be unravelled from the competing effects of  $Z^0$  exchange and a hyperfine correction and then interpreted in terms of a HWI model, e.g., the meson-exchange model of DDH.

Atomic PV has been measured in other systems but to lower precision than in Cs and with greater uncertainty in the atomic-structure details needed to interpret the measurements. Currently, a new generation of experiments is under development, aimed at determining both the nuclear spin-independent and anapole moment contributions to high precision. This includes ongoing efforts to develop alternative experimental approaches to atomic PV measurements in Cs; Guera and colleagues (79) recently reported on a new technique based on stimulated emission, anticipating that an ultimate precision of 0.1% could be reached. As remarked in Reference 80, there is a significant advantage to measuring PV in a range of isotopes of the same atom because a number of atomic-structure uncertainties cancel when PV ratios are considered. Researchers have proposed atomic ytterbium ( $Z = 70$ ), having seven stable isotopes (81), and preparatory spectroscopic studies are underway (82). Besides the atomic beam techniques described above, new experimental approaches based on trapped atoms or ions are also being explored (83, 84).

Perhaps the holy grail of this field is the study of atomic PV in radioactive Fr isotopes ( $Z = 87$ ), the heaviest alkali atomic system, recently reviewed in Reference 85. Both the spin-independent and anapole PV contributions are expected to be roughly an order of magnitude larger for Fr (depending on the isotope) than for Cs. In addition, Fr has a large number of isotopes spanning almost 30 neutrons, with lifetimes greater than 1 s, that cover a wide range of nuclear structure conditions, which in principle permits an unprecedented systematic study of atomic PV in a simple atomic system. With the longest-lived isotope  $^{223}\text{Fr}$  having a half-life of only 23 min, a radioactive beam facility is required for a future program of Fr PV studies. Pioneering atomic spectroscopy studies of a number of trapped Fr isotopes have been carried out at Stony Brook (86), and a collaboration has recently formed with the goal of establishing a long-term Fr program at the TRIUMF ISAC radioactive beam facility (87), where an actinide production target is planned and necessary to produce the required quantities of Fr (and other heavy systems of interest for fundamental symmetry tests such as proposed EDM measurements in radon).

**2.2.5. PARITY VIOLATION IN COMPOUND NUCLEI** In contrast to the extremely small ( $\simeq 10^{-7}$ ) PV asymmetries in the two-nucleon system, many-body nuclei have over the years provided numerous examples of parity violation on a much more significant scale, some of them surprisingly large (see e.g., Reference 9 and references therein). For the handful of cases for which reliable nuclear wavefunctions can be used to interpret the data, there is qualitative agreement with predictions of the meson-exchange model as illustrated in Figure 2, albeit with a

significant discrepancy in the scale of the pion coupling as discussed in Sections 1 and 2. Since the publication of Reference 9, an extensive and in many ways complementary program of PV measurements in compound nuclei has been carried out, dominated by the work of the TRIPLE collaboration at LANSCE. A review of this field was presented in this journal in 1993 (46), focusing on resonances in  $^{238}\text{U}$  and  $^{232}\text{Th}$ ; an updated comprehensive review of that and more recent data and analysis is provided in Reference 88.

The TRIPLE collaboration measured longitudinal cross-section asymmetries for neutron energies in the eV–keV range on a range of nuclear targets. Mixing of S- and P-wave resonances of the same J value leads to large PV effects in some cases, with enhancement factors as large as  $10^6$  relative to the NN PV asymmetries, resulting from the high density of states in the compound nucleus. The measurement of a number of PV asymmetries in the same nucleus is a key feature of this program, which is essential to the interpretation of the results. Using a statistical approach, the collaboration extracted results for either the RMS weak mixing matrix element  $M_J$  or the weak spreading width  $\Gamma_w = 2\pi M_J^2/D_J$ , where  $D_J$  is the level spacing, based on a total of 75 PV resonances observed in 18 nuclei. Important spectroscopic information (J values) for the resonant states was known in some cases and was modeled in other cases to interpret the results. The weak spreading widths were on the order of  $10^{-7}$  eV and roughly constant with mass number, whereas typical RMS matrix elements were on the scale of 1 meV.

Theoretical treatments have been developed that led to model predictions of the RMS matrix element based on an effective weak interaction with dominant isovector pion and isoscalar  $\rho$  exchange contributions taken from DDH predictions. A recent study by Tomsovic et al. (89) outlines a statistical spectroscopy approach for interpreting the experimental RMS matrix elements on the basis of PV asymmetry data from  $^{238}\text{U}$  and  $^{104,105,106,108}\text{Pd}$  targets to set limits on the weak meson-nucleon coupling constants. To date, a variety of theoretical approaches have been used to predict RMS matrix elements that are in qualitative agreement with experimental data on the basis of DDH predictions of the coupling constants, and which seem to favor a small value of  $h_\pi^1$  consistent with the  $^{18}\text{F}$  measurements shown in Figure 2, but a comprehensive program analyzing all the data to set limits on the weak coupling constants has not yet been attempted.

### 2.3. The End of the Road

Figures 2 and 7 summarize our present state of knowledge using the meson-exchange framework. We have reasonably clear experimental constraints on four linear combinations of the six weak meson-nucleon couplings from a mixture of few-nucleon and finite nuclear experiments, not all of which are in agreement with each other. The phenomenological implications of these results are unclear at best. On the one hand, the  $\vec{p}\vec{p}$  experiments now yield a rather stringent set of constraints on the combinations of the DDH couplings  $h_\rho^{PP}$  and  $h_\omega^{PP}$ , which govern the asymmetry over a fairly broad range of energy. As we discuss below,  $h_\rho^{PP}$  and  $h_\omega^{PP}$  essentially parameterize the contributions to  $A_z$  from the lowest-order,

short-range PV potential in the EFT. To the extent that the energy dependence of  $A_z$  is dominated by that of the strong interaction phase shifts that enter matrix elements of these operators as well as the unpolarized cross section,  $h_\rho^{pp}$  and  $h_\omega^{pp}$  need not be thought of as specific to the DDH meson-exchange framework.

On the other hand, the nuclear PV experiments are largely sensitive to two different combinations of the DDH parameters shown in Figure 2:  $h_S^{\text{nuc}} \equiv -(h_\rho^0 + 0.7h_\omega^0)$  and  $h_V^{\text{nuc}} \equiv h_\pi^1 - 0.12h_\rho^1 - 0.18h_\omega^1$  (7). In the past, it has been the conventional practice to project the constraints from the  $A_z$  measurements onto the  $h_{S,V}^{\text{nuc}}$  plane using the DDH theoretical ranges for the  $h_\rho^{1,2}$  and  $h_\omega^1$ . Here, however, we choose not to do so because we want to minimize the number of theoretical assumptions used in the extraction of information from experiment. Instead, we treat the nuclear experiments separately from the  $\vec{p}\vec{p}$  measurements. In the ideal situation, the analysis of the nuclear experiments would yield a self-consistent region for the  $h_{S,V}^{\text{nuc}}$ —a situation that clearly does not emerge from Figure 2. The primary problem seems to be the inclusion of the  $^{133}\text{Cs}$  anapole moment constraint, which finds no region of simultaneous consistency with all the other nuclear PV experiments. To explain this discrepancy, one might naturally re-examine the shell model calculation leading to the Cs band. However, theoretical considerations suggest that a more realistic calculation would lead to an even larger discrepancy (7, 24), whereas the results of more naive shell model computations (18, 19, 24, 25–30) lead to a similar result. Evidently, additional insight into the many-body physics of nuclear PV is needed before a consistent phenomenology can be obtained with the meson-exchange framework.

Even if such a consistent picture had emerged from experiment, extraction of fundamental information on the  $\Delta S = 0$  HWI would still be problematic. To explain why, we consider the physics embodied by the  $h_{S,V}^{\text{nuc}}$ . As compared with  $h_\rho^{pp}$  and  $h_\omega^{pp}$ , these effective nuclear couplings correspond to different combinations of the short-range EFT operators and long-range  $\pi$ -exchange PV potential than those that enter the  $\vec{p}\vec{p}$  asymmetry. However, the nuclear matrix elements of these operators sample the spatial dependence of both the operators as well as their action on the nuclear wavefunctions, and there is no simple way of disentangling the two as there is for the  $\vec{p}\vec{p}$  asymmetries.

To illustrate, we first consider the momentum-space form of the  $\rho$ - and  $\omega$ -exchange operators appearing in  $V_{\text{DDH}}^{\text{PV}}$ . Each term contains a pseudoscalar of the general form  $\vec{\sigma}_i \cdot \vec{p}_j$ , where the subscripts refer to nucleons  $i$  or  $j$ , times a function of the momentum transfer  $q = |\vec{q}|$  generated by the meson propagator in the static limit ( $q_0 = 0$ ) and a hadronic form factor  $F_{\rho,\omega}(q^2)$  arising from the meson-nucleon vertices

$$V_{V\text{-exchange}}^{\text{PV}} \sim \vec{\sigma}_i \cdot \vec{p}_j F_V(q^2) [1 + q^2/m_V^2]^{-1}. \quad 7.$$

For  $q \ll m_V$ , we may expand in powers of  $q^2/m_V^2$ :

$$V_{V\text{-exchange}}^{\text{PV}} \sim \vec{\sigma}_i \cdot \vec{p}_j F_V(0) \left( 1 + \frac{q^2}{m_V^2} [m_V^2 F'(0) - 1] + \dots \right), \quad 8.$$

where  $+\dots$  indicates higher-order terms. In a model-independent approach, the coefficient  $[m_V^2 F'(0) - 1]$  of the  $q^2/m_V^2$  term in Equation 8 would be replaced by an a priori unknown coefficient whose value would have to be taken from either an experiment or a QCD computation. A similar statement holds for the higher-order terms. At each order  $n$  in the expansion, additional pseudoscalar operators having a different structure than  $\vec{\sigma}_i \cdot \vec{p}_j (q^2/m_V^2)^n$  could also be included. In effect, the meson-exchange framework imposes model-dependent relations between all of the higher-order operator coefficients and those of the lowest-order terms—relations that may or may not hold in the SM.

The impact of the higher-order operators on nuclear matrix elements depends on both the values of the operator coefficients as well as the spatial dependence of the nuclear wavefunctions. Extraction of the  $h_{S,V}^{\text{nuc}}$  from experimental observables relies on both the relationships between these operators assumed implicitly by the meson-exchange model, as well as on nuclear model-space truncations and other nuclear structure inputs that affect the wavefunctions employed. At present, there is no rigorous way to disentangle the impact of either on the extracted PV couplings, and the constraints in Figure 2 may reflect both artifacts of nuclear structure calculations as well as assumed operator relations. In studying the fundamental  $\Delta S = 0$  HWI experimentally, it is best to avoid such an implicit reliance on model-dependent assumptions and nuclear structure inputs. Theoretically, the cleanest way to do so is to exploit EFT—wherein operator relations are determined systematically from experiment—and to study hadronic PV in few-body systems, for which ab initio theoretical computations are available.

### 3. EFFECTIVE FIELD THEORY FRAMEWORK

EFTs are ideally suited to situations in which a distinct hierarchy of scales exists. In the present instance, several scales are relevant: the weak scale  $v = (\sqrt{2}G_F)^{1/2} = 246$  GeV; the hadronic scale  $\Lambda_{\text{HAD}} \approx 1$  GeV; the pion mass and decay constants  $m_\pi \approx 140$  MeV and  $F_\pi = 93.2$  MeV, respectively; and the typical momentum  $Q$  relevant to a PV hadronic or nuclear process. The distance at which the repulsive core of the strong NN potential becomes dominant,  $r \lesssim 0.4$  fm, corresponds to a mass scale  $\gtrsim 500$  MeV, which, for our purposes, we take to be of order  $\Lambda_{\text{HAD}}$ . The size of hadronic matrix elements relevant to the HWI is governed by the ratio of  $F_\pi^2$  to  $v^2$ , which is typically normalized to the quantity  $g_\pi$ , as in Equation 4.

The remaining scales can be used to construct an effective Lagrangian out of nucleon and pion fields in which the operators are organized according to powers of  $Q/\Lambda$ . For processes in which  $Q \ll m_\pi$ , one should take  $\Lambda = m_\pi$ , treating the pions as heavy and “integrating them out” of the effective theory. For  $Q \gtrsim m_\pi$ , the pion must be kept as an explicit degree of freedom, and one should take  $\Lambda = \Lambda_{\text{HAD}}$ . Consequently, we consider two versions of the EFT corresponding to these two different regimes for  $Q$ .

### 3.1. The Pionless Effective Field Theory

In the PV EFT without pions, the lowest-order pseudoscalar operators contain four-nucleon fields and are  $\mathcal{O}(Q)$  because they must transform as  $\vec{\sigma}_i \cdot \vec{p}_j$ . At this order, there nominally exist 10 different contact operators. As shown in Reference 8, the most general short-range (SR) potential has the coordinate-space form

$$\begin{aligned}
 V_{1, \text{SR}}^{\text{PV}}(\vec{r}) = & \frac{2}{\Lambda^3} \left\{ \left[ C_1 + (C_2 + C_4) \left( \frac{\tau_1 + \tau_2}{2} \right)_3 + C_3 \tau_1 \cdot \tau_2 + \mathcal{I}_{ab} C_5 \tau_1^a \tau_2^b \right] \right. \\
 & (\vec{\sigma}_1 - \vec{\sigma}_2) \cdot \{-i\vec{\nabla}, f_m(r)\} \\
 & + \left[ \tilde{C}_1 + (\tilde{C}_2 + \tilde{C}_4) \left( \frac{\tau_1 + \tau_2}{2} \right)_3 + \tilde{C}_3 \tau_1 \cdot \tau_2 + \mathcal{I}_{ab} \tilde{C}_5 \tau_1^a \tau_2^b \right] \\
 & i(\vec{\sigma}_1 \times \vec{\sigma}_2) \cdot [-i\vec{\nabla}, f_m(r)] \\
 & + (C_2 - C_4) \left( \frac{\tau_1 - \tau_2}{2} \right)_3 (\vec{\sigma}_1 + \vec{\sigma}_2) \cdot \{-i\vec{\nabla}, f_m(r)\} \\
 & \left. + C_6 i \epsilon^{ab3} \tau_1^a \tau_2^b (\vec{\sigma}_1 + \vec{\sigma}_2) \cdot [-i\vec{\nabla}, f_m(r)] \right\}, \quad 9.
 \end{aligned}$$

where  $\mathcal{I}_{ab} = \text{diag}(1, 1, 2)$  and where the subscript 1 on  $V_{1, \text{SR}}^{\text{PV}}(\vec{r})$  indicates that this potential appears at  $\mathcal{O}(Q^1)$  in the EFT. Equation 9 has introduced the function  $f_m(\vec{r})$ , which is strongly peaked at about  $r = 0$  with some width  $\sim 1/m$  and which goes to  $\delta^{(3)}(\vec{r})$  in the zero-width ( $m \rightarrow \infty$ ) limit. For practical purposes, we will take  $1/m \lesssim 0.4 \text{ fm}$ .

At first glance, there appears to exist a dependence on 10 combinations of a priori unknown constants,  $C_{1-6}$  and  $\tilde{C}_{1-5}$ , that encode information about the short-distance weak interaction between two nucleons.<sup>4</sup> When considering processes with  $Q \ll m_\pi$ , however, not all of the operators in Equation 9 are independent. In this regime, PV observables are dominated by mixing between S- and P-waves, for which there exist only five independent spin-isospin amplitudes:

1.  $d_t(k)$ , representing  ${}^3S_1(I=0) - {}^1P_1(I=0)$  mixing;
2.  $d_s^{0,1,2}(k)$ , representing  ${}^1S_0(I=1) - {}^3P_0(I=1)$  mixing generated by  $I=0, 1, 2$  operators, respectively; and
3.  $c_t(k)$ , representing  ${}^3S_1(I=0) - {}^3P_1(I=1)$  mixing;

where we have used the notation of Danilov (90) and Desplanques & Missimer (10, 91). At the low energies relevant to the pionless EFT, the energy dependence of these amplitudes is dominated by the strong interaction phase shifts. Denoting the spin singlet and spin triplet strong interaction S-wave scattering amplitudes as

<sup>4</sup>The combination  $\tilde{C}_2 - \tilde{C}_4$  does not appear, so only 10 combinations of the 11 constants  $C_{1-6}$  and  $\tilde{C}_{1-5}$  are found in Equation 9.

$m_s(k)$  and  $m_t(k)$ , respectively, we have

$$\begin{aligned} ad_t(k) &= \lambda_t m_t(k) + \dots \\ d_s^i(k) &= \lambda_s^i m_s(k) + \dots \\ c_t(k) &= \rho_t m_t(k) + \dots, \end{aligned} \tag{10}$$

where  $+\dots$  indicates small corrections to the energy dependence arising from the strong P-wave phase shifts. Danilov's early formulation of the problem (90) argued for the forms in Equation 10, omitting the small corrections indicated. In the EFT framework, it is straightforward to derive the proportionality of the S-P amplitudes and the  $m_i(k)$  by computing the relevant T-matrix elements and summing up the strong rescattering contributions. In doing so, one finds that at low energies where P-wave rescattering contributions are small, the  $\lambda_i$  and  $\rho_t$  are given by the ratio of the lowest-order S-P scattering amplitude to the lowest-order, parity-conserving S-wave amplitude in a given spin-isospin channel (8).

The coefficients  $\lambda_t$ ,  $\lambda_s^i$ , and  $\rho_t$  are themselves proportional to various combinations of the  $C_i$  and  $\tilde{C}_i$  appearing in  $V_{1, \text{SR}}^{\text{PV}}(\vec{r})$ . In the zero-range ( $m \rightarrow \infty$ ) limit (8)<sup>5</sup>

$$\begin{aligned} \lambda_t &\propto (C_1 - 3C_3) - (\tilde{C}_1 - 3\tilde{C}_3) \\ \lambda_s^0 &\propto (C_1 + C_3) + (\tilde{C}_1 + \tilde{C}_3) \\ \lambda_s^1 &\propto (C_2 + C_4) + (\tilde{C}_2 + \tilde{C}_4) \\ \lambda_s^2 &\propto -\sqrt{8/3}(C_5 + \tilde{C}_5) \\ \rho_t &\propto \frac{1}{2}(C_2 - C_4) + C_6. \end{aligned} \tag{11}$$

In effect, at low energies, five of the operators in Equation 9 become redundant, leaving only five independent S-P amplitudes.

Inclusion of finite-range effects leads to modifications of these relations. Arriving at exact relations using state-of-the-art NN potentials remains an unfinished task for many-body theorists. However, we provide approximate expressions by drawing on the work of Desplanques & Benayoun (92). We obtain

$$\begin{aligned} m_N \lambda_t &= -\frac{2}{\Lambda^3} [B_4(C_1 - 3C_3 + \tilde{C}_1 - 3\tilde{C}_3) + B_5(C_1 - 3C_3 - \tilde{C}_1 + 3\tilde{C}_3)] \\ m_N \lambda_s^0 &= -\frac{2}{\Lambda^3} [B_6(C_1 + C_3 + \tilde{C}_1 + \tilde{C}_3) + B_7(C_1 + C_3 - \tilde{C}_1 - \tilde{C}_3)] \\ m_N \lambda_s^1 &= -\frac{2}{\Lambda^3} [B_6(C_2 + C_4 + \tilde{C}_2 + \tilde{C}_4) + B_7(C_2 + C_4 - \tilde{C}_2 - \tilde{C}_4)] \end{aligned}$$

<sup>5</sup>The last equation of Equation 46 in Reference 8 contains an error. The sign in front of  $C_6$  should be  $+$  rather than  $-$ .

$$\begin{aligned}
m_N \lambda_s^2 &= \frac{4\sqrt{6}}{\bar{\Lambda}^3} [B_6(C_5 + \tilde{C}_5) + B_7(C_5 - \tilde{C}_5)] \\
m_N \rho_t &= -\frac{2}{\bar{\Lambda}^3} \left[ B_2 \left( \frac{1}{2} C_2 - \frac{1}{2} C_4 + C_6 \right) + B_3 \left( \frac{1}{2} C_2 - \frac{1}{2} C_4 - C_6 \right) \right], \quad 12.
\end{aligned}$$

where  $\bar{\Lambda} = m_N m_\rho^2 / \Lambda^3$  and where the  $B_k$  are linear combinations of the  $\beta_{ij}^\pm$  of Reference 92. For example, using the values of those constants obtained with the Reid Soft Core potential, we obtain  $B_k = (-0.0043, 0.0005, -0.0009, -0.0022, -0.0067, 0.0003)$  for  $k = 2 \dots 7$ , respectively.<sup>6</sup>

The coefficients  $B_{2,5,6}$  multiply the combinations of  $C_i$  and  $\tilde{C}_i$  expected to arise in the lowest-order EFT (Equation 11). The remaining terms are generated by finite-range contributions that occur beyond LO. Although we have not included the full set of PV operators and amplitudes that occur at next-to-leading order (NLO), the magnitudes of the  $B_{3,4,7}$  relative to the  $B_{2,5,6}$  indicate the magnitude of higher-order effects and of the error associated with working to lowest order. The Reid Soft Core values obtained in Reference 92 give  $|B_3/B_2| = 0.12$ ,  $|B_4/B_5| = 0.41$ , and  $|B_7/B_6| = 0.04$ , suggesting that in general the impact of neglected higher-order contributions is small except in the case of  $\lambda_t$ .

Before considering the application of this framework to specific observables, it is useful to obtain theoretical predictions for the quantities  $\rho_t$  and  $\lambda_{s,t}$ . To that end, we first consider the correspondence with the DDH meson-exchange model and delineate the relationship between the  $C_i$  and  $\tilde{C}_i$  and the DDH parameters. Using

$$f_m(\vec{r}) = \frac{m^2}{4\pi r} \exp(-mr), \quad 13.$$

with  $m$  being the parameter that defines the range of the PV potential, and letting

$$\bar{\Lambda}_V^3 \equiv \frac{\Lambda^3}{m_N m_M^2} \quad 14.$$

for  $M = \rho, \omega$ , we obtain<sup>7</sup>

$$\begin{aligned}
C_1^{\text{DDH}} &= -\frac{1}{2} \bar{\Lambda}_\omega^3 g_\omega h_\omega^0 & C_2^{\text{DDH}} &= -\frac{1}{2} \bar{\Lambda}_\omega^3 g_\omega h_\omega^1 \\
C_3^{\text{DDH}} &= -\frac{1}{2} \bar{\Lambda}_\rho^3 g_\rho h_\rho^0 & C_4^{\text{DDH}} &= -\frac{1}{2} \bar{\Lambda}_\rho^3 g_\rho h_\rho^1
\end{aligned}$$

<sup>6</sup>The expressions in Equation 12 are applicable to the EFT without pions. For a discussion of the modifications due to inclusion of explicit pions, see Section 3.2. In particular, the lowest-order contribution from single pion exchange appears in  $\rho_t$ .

<sup>7</sup>The corresponding expressions given in equation 141 of Reference 8 contain typographical errors. The quantity  $\Lambda_V$  should contain only two powers of  $m_M$  in the denominator, and each of the  $C_i$  should be proportional to the product of a strong coupling  $g_M$  and the relevant  $h_M^i$  as in Equations 14–16 here.

$$C_5^{\text{DDH}} = \frac{1}{4\sqrt{6}} \bar{\Lambda}_\rho^3 g_\rho h_\rho^2 \quad C_6^{\text{DDH}} = -\frac{1}{2} \bar{\Lambda}_\rho g_\rho h_\rho^1 \quad 15.$$

and

$$\begin{aligned} \frac{\tilde{C}_i^{\text{DDH}}}{C_i^{\text{DDH}}} &= 1 + \chi_\omega \quad i = 1, 2, \\ \frac{\tilde{C}_i^{\text{DDH}}}{C_i^{\text{DDH}}} &= 1 + \chi_\rho \quad i = 3 - 5. \end{aligned} \quad 16.$$

Using Equations 15 and 16, the expressions for  $\rho_t$ ,  $\lambda_t$ , and  $\lambda_s^{0,1,2}$  can easily be obtained, and the DDH best values and reasonable  $\lambda$  ranges for the PV meson-nucleon couplings can be employed to obtain the predictions for the PV LECs listed in Table 2. The results in columns 2–4 were obtained by retaining only the combinations of the  $C_i$ ,  $\tilde{C}_i$  that arise at lowest order in the EFT. Column 5 contains estimates of the size of higher-order contributions, which are based on the DDH best values for the  $C_i$ ,  $\tilde{C}_i$  and the terms in Equation 12 proportional to  $B_{3,4,7}$ .

To obtain a sense of the possible variations in theoretical predictions for the PV LECs from their correspondence with the DDH parameterization, we consider two approaches. First, we vary the values of the strong couplings in Equation 15 in accordance with the Bonn one-pion-exchange potential as suggested by Miller (93). As indicated in Table 2, doing so changes both the overall magnitude of the  $C_i$  and  $\tilde{C}_i$ , as well as the relation between the two, and leads in general to wider ranges for the PV LECs than those obtained with the values of the strong couplings originally used by DDH. Second, we give expectations using naive dimensional analysis (NDA) considerations, as discussed in Section 3.2 below. The NDA arguments suggest that the magnitudes of the  $C_i$  and  $\tilde{C}_i$  ought to be of order  $16\pi^2 \sim 150$ , but do not fix the signs of the  $C_i$  and  $\tilde{C}_i$ . To translate the NDA estimates into predictions for the five LECs, we simply take the magnitudes of the combinations of  $C_i$  and  $\tilde{C}_i$  appearing in Equation 12 to be the NDA expectation for any one of them.

**TABLE 2** Predictions for the five PV LECs characterizing hadronic PV in the pionless EFT

PV LEC	DDH best value	DDH range	DDH plus Bonn	Higher order	NDA
$m_N \rho_t$	0.05	0.07 $\rightarrow$ 0.03	0.18 $\rightarrow$ 0.08	$\pm 0.006$	$\pm 0.38$
$m_N \lambda_t$	0.84	-1.00 $\rightarrow$ 2.48	-2.44 $\rightarrow$ 6.12	$\pm 1.2$	$\pm 0.31$
$m_N \lambda_s^0$	3.82	-4.86 $\rightarrow$ 11.7	-9.84 $\rightarrow$ 22.96	$\pm 0.09$	$\pm 0.64$
$m_N \lambda_s^1$	0.37	0.64 $\rightarrow$ 0.21	1.53 $\rightarrow$ 0.54	$\pm 0.0006$	$\pm 0.64$
$m_N \lambda_s^2$	2.72	2.17 $\rightarrow$ 3.15	3.83 $\rightarrow$ 5.55	$\pm 0.06$	$\pm 3$

All values are quoted in units of  $g_\pi = 3.8 \times 10^{-8}$ . Estimates are obtained using Reid Soft Core potential, as in Reference 92; DDH values are taken from Reference 6.

In obtaining the correspondence between the PV LECs and the DDH predictions in the meson-exchange model, we have not included contributions from the parameter  $h_\rho^{1'}$  that appears in  $V_{\text{DDH}}^{\text{PV}}$ . Using the estimate of Reference 15 for this parameter would increase the magnitude of  $\rho_t$  appearing in Table 2, although not substantially. Generally, analyses of hadronic PV using the meson-exchange model have neglected this parameter because its contribution to  $V_{\text{DDH}}^{\text{PV}}$  has the same spin-isospin structure as for the  $\pi$ -exchange contribution but is suppressed by its short range. In the EFT framework, this term corresponds to the operator proportional to  $C_6$  that, in addition to  $C_{2,4}$ , contributes to  $\rho_t$ . Because the coefficients of  $C_{2,4,6}$  in  $\rho_t$  have comparable magnitude, we see no model-independent reason to neglect the  $C_6$  contribution in the most general analysis.

With the foregoing set of benchmarks in hand, it is instructive to consider the dependence of various few-body PV observables on the  $\lambda_i$  and  $\rho_t$  and to outline a program of high-precision measurements that could be used to determine these parameters. The few-body PV observables of interest include

1. polarized  $\vec{p}p$  scattering at 13.6 and 45 MeV, yielding the asymmetry  $A_z^{pp}$ ;
2. polarized  $\vec{p}\alpha$  scattering at 46 MeV, giving  $A_z^{p\alpha}$ ;
3. radiative  $\vec{n}p$  capture at low energy:  $\vec{n}p \rightarrow d\gamma$ , yielding the photon asymmetry  $A_\gamma^d$ ;
4. radiative  $np$  capture with unpolarized neutrons, giving the photon circular polarization  $P_\gamma^d$ , or alternatively, the asymmetry  $A_L^\gamma$  in  $\vec{\gamma}d \rightarrow np$ ;
5. rotation through an angle  $\phi$  about the momentum direction of polarized neutron spin passing through  ${}^4\text{He}$ , from which one extracts the quantity  $d\phi^{n\alpha}/dz$ ; and
6. radiative capture of polarized neutrons on deuterium at threshold  $\vec{n}d \rightarrow t\gamma$ , yielding the photon asymmetry  $A_\gamma^t$ .

Explicit expressions for these quantities in terms of the S-P amplitude parameters have been given in References 10, 91, and elsewhere. Table 3 gives coefficients of the five PV LECs as they appear in various observables. Theoretical expectations for these observables in the pionless EFT can be obtained using Tables 2 and 3. These expectations will, in general, differ when going to the EFT with explicit pions discussed in Section 3.2. In particular, the parameter  $m_N\rho_t$  that governs the asymmetry  $A_\gamma^d$  will be dominated by LO pion exchange, assuming  $h_\pi^1$  has its natural size. Table 3 also shows the most precise experimental results published to date for these observables. Notably, only  $A_z^{pp}$  and  $A_z^{p\alpha}$  have been measured to sufficient precision to establish a nonzero PV effect that can constrain the PV LECs. A review of recent, ongoing, and prospective efforts to obtain precision measurements of these important few-body PV effects appears in Section 3.4 below.<sup>8</sup>

<sup>8</sup>The measurement of  $P_\gamma^d$  is particularly challenging because of the limited sensitivity of conventional  $\gamma$ -ray circular polarimeters in the  $\sim$  MeV energy range; an alternative measurement of  $A_L^\gamma$  close to threshold yields the same physics and may be more accessible

TABLE 3 Sensitivities of selected PV observables to the five PV LECs

Observable	$m_N \rho_t$	$m_n \lambda_t$	$m_N \lambda_s^0$	$m_N \lambda_s^1$	$m_N \lambda_s^2 / \sqrt{6}$	Experiment ( $10^{-7}$ )	Reference
$A_z^{pp}(k)$	0	0	$4k/m_N$	$4k/m_N$	$4k/m_N$	$-0.93 \pm 0.21$ $-1.50 \pm 0.22$	(143) (144)
$A_z^{p\alpha}$	-1.07	-0.54	-0.72	-0.48	0	$-3.3 \pm 0.9$	(145)
$P_\gamma$	0	0.63	-0.16	0	0.32	$1.8 \pm 1.8$	(62)
$A_\gamma^d$	-0.107	0	0	0	0	$0.6 \pm 2.1$	(64)
$d\phi^{n\alpha}/dz$	-2.68	1.34	1.8	-1.2	0	$8 \pm 14$	(75)
$A_\gamma^t$	-3.56	-1.39	-0.95	-0.24	1.18	$42 \pm 38$	(146)

The first column gives the observable, and subsequent columns give the coefficients of a given PV LEC. For the  $pp$  asymmetry,  $k$  is the incident proton momentum in the lab frame. The final columns give the most precise experimental limits to date and their references; for the  $pp$  case, we quote the 13.6 and 45 MeV measurements, to which the lowest-order EFT best applies. Note that the  $p\alpha$  asymmetry is evaluated at 46 MeV;  $d\phi^{n\alpha}/dz$  is evaluated in rad/m.

The longitudinal asymmetry  $A_z^{pd}$  in  $\vec{p}d$  scattering was measured to high precision at 43 MeV (94, 95) in the 1980s but remains to be analyzed in a theoretical framework accounting for PV in both elastic scattering and breakup channels, both of which contributed to the experimental signal. There are also several possibilities for few-body experiments for which we have not yet obtained expressions for the PV observables in terms of the PV LECs. These include measurements of PV neutron spin rotation on hydrogen,  $d\phi^{np}/dz$ , and deuterium,  $d\phi^{nd}/dz$ , and one could also consider the circular polarization  $P_\gamma^t$  in  $nd \rightarrow t\gamma$  as well as perhaps the transmission asymmetry of unpolarized neutrons through polarized  ${}^3\text{He}$ . With realistic prospects for performing some or all of these measurements in the future, deriving the appropriate expressions is clearly important.

3.1.1. LIMITS OF THE PIONLESS EFFECTIVE FIELD THEORY Before discussing the EFT with pions, it is instructive to investigate the limits of validity of the pionless theory by considering the low-energy  $\vec{p}\vec{p}$  asymmetry as an illustrative example. Again, considering only S-P mixing, it is straightforward to show that (8)

$$A_z^{pp} = \frac{\sigma_+ - \sigma_-}{\sigma_+ + \sigma_-} = \frac{4k \operatorname{Re}[m_s^*(k)d_s^{pp}(k)]}{|m_s(k)|^2} \simeq 4k\lambda_s^{pp}, \quad 17.$$

where we have neglected small corrections arising from the P-wave phase shifts as before. A more complete decomposition of  $A_z^{pp}$  in terms of higher partial waves was first worked out by Simonius (47) and subsequently studied by several authors. A recent analysis using state-of-the-art NN potentials was performed in Reference 58 and used to extract the DDH parameters  $h_\rho^{pp}$  and  $h_\omega^{pp}$ .

to experiment. A possible experiment is in its early stages of development in Athens (69), as mentioned in Section 2.2, but is not discussed further in Section 3.4.

Following Simonius' original formulation, the asymmetry may be written as

$$A_z^{pp} = \sum_{\text{even } J} f_{J\pm}(E) K_{J\pm}(E, \theta), \quad 18.$$

where  $\pm$  indicates the orbital angular momentum  $L = J \pm 1$  and where  $E$  and  $\theta$  are the energy and scattering angle, respectively.  $f_{J\pm}$  are reduced PV transition amplitudes and  $K_{J\pm}$  contain all the dependence on the strong phases that arise from rescattering. For the  $J = 0$  partial wave, only  $f_{0+}$  exists, and it is proportional to the combination  $d_s^{pp}$  of the S-P amplitudes  $d_s^i$  that enter the  $\vec{p}\vec{p}$  process:

$$d_s^{pp} = -2if_{0+} \exp i[\delta(^1S_0) + \delta(^3P_0)]. \quad 19.$$

To the extent that the finite (but short) range of the PV potential may be neglected,  $d_s^{pp}$  and  $f_{0+}$  are proportional to  $\lambda_s^{pp}$ . Moreover, in obtaining Equation 17, we have neglected the dependence of  $d_s^{pp}$  on  $\delta(^3P_0)$ . Doing so is equivalent to taking  $K(E, \theta) \propto k$ .

Although this approximation holds to a high degree of accuracy for low-energy interactions, it breaks down for  $E \sim 100$  MeV ( $k \sim 300$  MeV). Because of cancellations between the effects of the S- and P-wave phase shifts in  $d_s^{pp}$  that occur above this energy, the contribution of the  $J = 0$  partial wave to  $A_z^{pp}$  falls rapidly, reaching zero at  $E = 227$  MeV. Moreover, the contribution from the  $J = 2$  partial wave—dominated by the  $^1D_2 - ^3P_2$  ( $f_{2-}$ ) mixing—becomes appreciable. Taking advantage of the former, the beam energy for the TRIUMF  $A_z^{pp}$  (221 MeV) measurement was optimized, accounting for finite acceptance of the apparatus, to ensure that the  $f_{0+}$  contribution was entirely cancelled so that the asymmetry was determined almost entirely by the  $f_{2-}$  contribution (48, 58). Thus, a combined analysis of the TRIUMF and lower-energy  $A_z^{pp}$  measurements yields constraints on the two amplitudes  $f_{0+}$  and  $f_{2-}$ . In effect, the values of  $h_\rho^{pp}$  and  $h_\omega^{pp}$  obtained in Reference 58 may be treated as equivalent parameterizations of these two partial wave transition amplitudes and are not necessarily specific to the meson-exchange framework.

Clearly, at the energies of the recent TRIUMF experiment, the lowest-order EFT is no longer applicable, and  $\mathcal{O}(Q^3)$  operators in  $V_{SM}^{PV}$  that characterize P-D mixing must be included. Doing so introduces a host of new, a priori unknown operator coefficients. In addition, the redundancy of operators in the  $\mathcal{O}(Q)$   $V_{SR}^{PV}$  in Equation 9, which holds for the S-P amplitudes, breaks down, and all 10 lowest-order operators become independent. Determining all of these constants from experiment would be unrealistic, so we restrict our attention to the energy range in which the lowest-order EFT applies.

### 3.2. Parity-Violating Effective Field Theory with Pions

For PV processes involving few-body nuclei, the relevant energy scale  $Q$  is no longer set solely by experimental kinematics; it also includes the relevant internal momentum of the bound nucleons. Because the latter can be as large as the Fermi

momentum of  $\gtrsim 200$  MeV, it is no longer reasonable to treat the pion as heavy. For decades, phenomenological strong interaction potentials for light nuclei have included a long-range  $\pi$ -exchange component. For the EFT formulation, treating pionic contributions consistently has presented challenges. The difficulty arises from the presence of two-nucleon poles in iterated  $\pi$ -exchange amplitudes whose contributions are enhanced by  $\sim m_N/Q$  relative to naive expectations. These enhanced contributions spoil the power counting in  $Q/\Lambda$ , which is essential to the success of the EFT approach. Thus, strong pion exchange must be summed to all orders to obtain a consistent treatment. Indeed, as shown in Reference 96, treating the pion perturbatively, as done in the framework of References 97 and 98, does not lead to a convergent expansion in all channels of the NN interaction.

An alternate formulation, originally proposed by Weinberg (99, 100), entails performing the all-orders resummation in terms of the effective strong potential. To be self-consistent, however, it appears that the EFT expansion of the potential about the chiral limit (101–103)  $m_\pi = 0$  must be performed simultaneously, because a full resummation of the chiral symmetry-breaking component of the one-pion-exchange potential leads to inconsistent renormalization (97, 98, 101–103). Although the chiral-expansion treatment of the Weinberg approach is still under development, we follow Reference 8 and employ it here.

The basis for the EFT with pions is  $\chi$ PT, whose formalism is well known and will not be repeated here. However, we note that its formulation for hadronic PV processes was first worked out by Kaplan & Savage (104), whose notation follows. The nonlinear dependence of the effective Lagrangian on the pion is implemented via the field

$$\xi = \exp\left(\frac{i\pi^a \tau^a}{2F_\pi}\right), \quad 20.$$

where  $\pi^a$  ( $a = 1, 2, 3$ ) are the isospin components of the pion field. Defining the quantity

$$X_-^3 = \xi^\dagger \tau^3 \xi - \xi \tau^3 \xi^\dagger, \quad 21.$$

the lowest-order Lagrangian for a PV interaction of the pion with a single nucleon is

$$\begin{aligned} \mathcal{L}_{\pi N, \text{PV}}^{(-1)} &= -\frac{h_\pi^1}{2\sqrt{2}} \bar{N} X_-^3 N \\ &= -ih_\pi^1 (\bar{p} n \pi^+ - \bar{n} p \pi^-) + \dots, \end{aligned} \quad 22.$$

where  $+\dots$  indicates the higher-order terms in odd powers of  $(\pi^a \tau^a / F_\pi)$  that arise from expanding the exponential in  $\xi$ . The leading term in the Lagrangian in Equation 22 is identical to the PV Yukawa interaction in the DDH model. Consequently, its contribution to the PV NN potential is the same as the first term

in Equation 2:

$$V_{(-1,\text{LR})}^{\text{PV}}(\vec{r}) = i \frac{h_\pi^1 g_A m_N}{\sqrt{2} F_\pi} \left( \frac{\vec{\tau}_1 \times \vec{\tau}_2}{2} \right)_3 (\vec{\sigma}_1 + \vec{\sigma}_2) \cdot \left[ \frac{\vec{p}_1 - \vec{p}_2}{2m_N}, w_\pi(r) \right]. \quad 23.$$

The subscript  $-1$  indicates that this long-range (LR) potential is  $\mathcal{O}(Q^{-1})$ , a feature most readily seen from its momentum-space form:

$$V_{(-1,\text{LR})}^{\text{PV}}(\vec{q}) = -i \frac{g_A h_\pi^1}{\sqrt{2} F_\pi} \left( \frac{\vec{\tau}_1 \times \vec{\tau}_2}{2} \right)_3 \frac{(\vec{\sigma}_1 + \vec{\sigma}_2) \cdot \vec{q}}{q^2 + m_\pi^2}, \quad 24.$$

where  $\vec{q} = \vec{p}_1 - \vec{p}_1' = \vec{p}_2' - \vec{p}_2$  is the three-momentum of the exchanged pion,  $\vec{p}_i$  ( $\vec{p}_i'$ ) is the initial (final) momentum of nucleon  $i$ , and  $q = |\vec{q}|$ .

Because the PV potential must transform as a pseudoscalar, the operators in it contain odd numbers of derivatives. Thus, the subleading terms are expected to be  $\mathcal{O}(Q)$ , as in  $V_{(1,\text{SR})}^{\text{PV}}$ . In principle, loop corrections to the Lagrangian (Equation 22) or to  $V_{(-1,\text{LR})}^{\text{PV}}(\vec{r})$  could bring in a factor of  $m_\pi$  or  $p^2/m_\pi$ , leading to an  $\mathcal{O}(Q^0)$  component. Explicit computations, however, indicate that no such contributions exist. Consequently, the subleading components of the potential start off at  $\mathcal{O}(Q)$  (next-to-next-to-leading order, NNLO), and it is convenient to distinguish them according to their range:

1. Short range:  $V_{(1,\text{SR})}^{\text{PV}}$  as in Equation 9 but with  $\Lambda = \Lambda_{\text{HAD}} \approx \Lambda_\chi = 4\pi F_\pi$ .
2. Medium range:  $V_{(1,\text{MR})}^{\text{PV}}$ , generated by the two-pion exchange diagrams of Figure 1c and proportional to  $h_\pi^1$ . The structure of the operator is most conveniently given in momentum space, as it carries a nonanalytic dependence on pion momentum and mass (8):

$$V_{(1,\text{MR})}^{\text{PV}}(\vec{q}) = -\frac{1}{\Lambda_\chi^3} \left\{ \tilde{C}_2^{2\pi}(q) \frac{\tau_1^z + \tau_2^z}{2} i(\vec{\sigma}_1 \times \vec{\sigma}_2) \cdot \vec{q} + C_6^{2\pi}(q) i \epsilon^{ab3} [\vec{\tau}_1 \times \vec{\tau}_2]_3 (\vec{\sigma}_1 + \vec{\sigma}_2) \cdot \vec{q} \right\}, \quad 25.$$

where (see Note Added in Proof)

$$\begin{aligned} \tilde{C}_2^{2\pi}(q) &= -8\sqrt{2}\pi g_A^3 h_\pi^1 L(q) \\ C_6^{2\pi}(q) &= -\sqrt{2}\pi g_A h_\pi^1 L(q) + \sqrt{2}\pi [3L(q) - H(q)] g_A^3 h_\pi^1, \end{aligned} \quad 26.$$

and

$$\begin{aligned} L(q) &= \frac{\sqrt{4m_\pi^2 + q^2}}{q} \ln \left( \frac{\sqrt{4m_\pi^2 + q^2} + q}{2m_\pi} \right), \\ H(q) &= \frac{4m_\pi^2}{4m_\pi^2 + q^2} L(q). \end{aligned} \quad 27.$$

3. Long range:  $V_{(1,LR)}^{PV}$ , generated by one-loop corrections to the PV  $\pi NN$  Yukawa and parity-conserving strong vertices, as well as by additional operators having a distinct structure from the lowest-order potential. However, the impact of all of the NNLO PV operators can be absorbed into  $V_{(-1,LR)}^{PV}$  and  $V_{(1,SR)}^{PV}$  through a suitable redefinition of the operator coefficients. The remaining PC operators give rise to the momentum-space potential (8)

$$\begin{aligned}
 V_{i,LR}^{PV}(\vec{p}_1, \dots, \vec{p}_2') &= +i \frac{g_A h_\pi^1}{\sqrt{2} m_N^2 F_\pi} \left( \frac{\vec{\tau}_1 \times \vec{\tau}_2}{2} \right)_3 \frac{1}{q^2 + m_\pi^2} \\
 &\quad \left\{ \frac{1}{4} [(|\vec{p}_1|^2 - |\vec{p}_1'|^2) \vec{\sigma}_1 \cdot (\vec{p}_1' + \vec{p}_1) - (1 \leftrightarrow 2)] \right. \\
 &\quad - \frac{1}{8} [(|\vec{p}_1|^2 + |\vec{p}_1'|^2) \vec{\sigma}_1 \cdot \vec{q} + (1 \leftrightarrow 2)] \\
 &\quad \left. + \frac{1}{4} [\vec{\sigma}_1 \cdot \vec{p}_1' \vec{q} \cdot \vec{p}_1 + \vec{\sigma}_1 \cdot \vec{p}_1 \vec{q} \cdot \vec{p}_1' + (1 \leftrightarrow 2)] \right\}, \quad 28.
 \end{aligned}$$

where  $\vec{q}_i = \vec{p}_i' - \vec{p}_i$  and  $k_\pi^{1a}$  is a constant that must be determined from experiment.

In addition to considering the potential through  $\mathcal{O}(Q)$ , two-body current operators that contribute to the same order when considering PV processes involving photons must also be included. These operators include the standard PV meson-exchange currents associated with the  $\pi$ -exchange potential and those arising from the covariant derivatives in  $V_{(1,SR)}^{PV}$ . In addition, there exists a new, independent current operator (8)

$$\vec{J}(\vec{x}_1, \vec{x}_2, \vec{q}) = \frac{\sqrt{2} g_A \bar{C}_\pi m_\pi^2}{\Lambda^2 F_\pi} e^{-i\vec{q} \cdot \vec{x}_1} \tau_1^+ \tau_2^- \vec{\sigma}_1 \times \vec{q} \vec{\sigma}_2 \cdot \hat{r} H_\pi(r) + (1 \leftrightarrow 2), \quad 29.$$

where

$$H_\pi(r) = \frac{\exp(-m_\pi r)}{m_\pi r} \left( 1 + \frac{1}{m_\pi r} \right), \quad 30.$$

and  $\bar{C}_\pi$  is an additional LEC parameterizing the leading PV  $NN\pi\gamma$  interaction.

**3.2.1. PARITY-VIOLATING EFFECTIVE FIELD THEORY WITH PIONS: NEW FEATURES** In comparison with the DDH meson-exchange potential, the EFT with explicit pions introduces several qualitatively distinct features. First, the  $\mathcal{O}(Q)$  long-range operators in Equations 28 and 29 have no analog in the DDH framework and introduce one unknown constant,  $\bar{C}_\pi$ . Given the novel nature of these operators, the impact of their contributions to the observables discussed above has yet to be determined with explicit, few-body computations. On the basis of the isospin

structure of these two operators, however, they should contribute to the same processes, such as  $\vec{n}\vec{p} \rightarrow d\gamma$ , that are sensitive to the LO  $\pi$ -exchange potential. Power counting implies that the magnitude of their contribution should be smaller than that of  $V_{(-1, \text{LR})}^{\text{PV}}$ , but their long-range character suggests that they should have a greater impact than the operators in  $V_{(1, \text{SR})}^{\text{PV}}$ . Future few-body calculations should test these expectations.

The TPE medium-range potential  $V_{(1, \text{MR})}^{\text{PV}}$  is similarly a new feature of the EFT framework. In the past, others have attempted to introduce PV TPE using model frameworks (see e.g., Reference 105), but to our knowledge, the result in Equation 26 gives the first model-independent formulation that is consistent with the symmetries of QCD. The operator coefficients  $\tilde{C}_2^{2\pi}$  and  $C_6^{2\pi}$  have been labeled to indicate their correspondence with the operators in  $V_{(1, \text{SR})}^{\text{PV}}$ , but as indicated in Equation 26, the coefficients are fixed in terms of  $h_\pi^1$  and are not independent free parameters. The operator proportional to  $C_6^{2\pi}$  has the same isospin structure as  $V_{(-1, \text{LR})}^{\text{PV}}$  and contributes to any process—such as  $\vec{n}\vec{p} \rightarrow d\gamma$ —that is sensitive to the LO  $\pi$ -exchange potential. The operator proportional to  $\tilde{C}_2^{2\pi}$  has the same structure as the  $h_\omega^1(1 + \chi_\omega)$  term in the DDH potential and therefore generates a medium-range contribution to any observable sensitive to the latter combination in the meson-exchange model. In particular, this operator contributes to both the  $f_{0^+}$  and  $f_{2^-}$  partial wave terms in  $A_z^{pp}$ , implying that this observable is sensitive to  $h_\pi^1$  and short-range effects at the same order in  $Q$ . In either case, proper inclusion of the TPE medium-range potential will affect the determination of  $h_\pi^1$  obtained from a global analysis of few-body PV observables.

In principle, three-body PV forces that arise in the EFT with pions should also be taken into account, as we go on to discuss few-body experiments in systems involving three or more nucleons. As discussed in Reference 8, three-body PV forces do not arise at  $\mathcal{O}(Q)$ , so we restrict our attention to the two-body PV EFT interaction.

### 3.2.2. PARITY-VIOLATING LOW-ENERGY CONSTANTS: NAIVE DIMENSIONAL ANALYSIS

Beyond these qualitative observations, we cannot make any quantitative statements regarding the relative importance of the new features of the PV EFT with pions. Evaluating their contributions to specific observables now constitutes an open problem for few-body theorists. However, it is instructive to estimate the size of the constants  $C_i$ ,  $\tilde{C}_i$ ,  $h_\pi^1$ , and  $\tilde{C}_\pi$ , which arise in the EFT. Manohar & Georgi (106) developed a systematic way of doing so, NDA, that has successfully explained the size of a variety of LECs in  $\chi$ PT. According to NDA, operators should be constructed by scaling fields and derivatives to their natural scales:

$$\left(\frac{D_\mu}{\Lambda_\chi}\right)^d \left(\frac{\pi}{F_\pi}\right)^p \left(\frac{\bar{N}N}{\Lambda_\chi F_\pi^2}\right)^{f/2} \times (\Lambda_\chi F_\pi)^2 \times (g_\pi)^n, \quad 31.$$

where  $d, p, f = 2k$ ;  $k$  and  $n$  are positive integers; and  $g_\pi$  is as given in Equation 4. Consequently, PV LECs are expected to have the magnitudes

$$h_\pi^1 \sim \left( \frac{\Lambda_\chi}{F_\pi} \right) g_\pi \sim 10g_\pi \quad 32.$$

$$C_i, \tilde{C}_i \sim \left( \frac{\Lambda_\chi}{F_\pi} \right)^2 g_\pi \sim 100g_\pi \quad 33.$$

$$\bar{C}_\pi = g_\pi \sim g_\pi. \quad 34.$$

It is interesting that because  $\Lambda_\chi/F_\pi = 4\pi \sim 12$ , the NDA estimates for  $h_\pi^1$  and the  $C_i, \tilde{C}_i$  are roughly equal to the expectations based on correspondence with the DDH best values. In contrast, the new long-range LEC,  $\bar{C}_\pi$ , is expected to be an order of magnitude smaller than  $h_\pi^1$ . This difference, however, simply reflects the conventions used above in normalizing the various operators.

**3.2.3. PARITY-VIOLATING EFFECTIVE FIELD THEORY: PHENOMENOLOGY** The phenomenology of the PV EFT with pions is clearly more challenging than for the pionless theory, as one encounters additional unknown parameters when working to  $\mathcal{O}(Q)$  and because a variety of new contributions remain to be computed. In principle, there exists a viable experimental program that could determine the constants to this order, including the six measurements highlighted in Section 3.1 for the pionless theory plus one additional, independent experiment. As noted in Section 3.1, possibilities for the latter include a careful analysis of the  $\bar{p}d$  scattering asymmetry results for  $A_z^{pd}$  (94, 95) and future neutron spin rotation measurements on hydrogen or deuterium. Recently, the possibility of performing PV photo- and electroproduction experiments on a single nucleon to determine the values of the PV  $\pi N$  and  $\gamma N$  couplings has received considerable attention. Carrying out these experiments, which we discuss below, would provide additional, independent input for the determination of the PV LECs.

Theoretically, the extraction of these constants from experiment will require new calculations to determine the contributions from (a) the medium-range, TPE potential (Equation 25), (b) the NNLO single pion-exchange potential (Equation 28), and (c) the meson-exchange current (Equation 29). At present, only the dependence on  $h_\pi^1$  generated by LO pion exchange is known:

$$m_N \rho_t = 1.04 h_\pi^1 + m_N \rho_t^{\text{SR}} + m_N \Delta \rho_t, \quad 35.$$

where  $\rho_t^{\text{SR}}$  gives the dependence of the  ${}^3S_1$ - ${}^3P_1$  mixing on the constants appearing in  $V_{1,\text{SR}}^{\text{PV}}$  as in Equation 12,  $\Delta \rho_t$  gives the presently unknown contributions generated by  $V_{1,\text{MR}}^{\text{PV}}$  and  $V_{1,\text{LR}}^{\text{PV}}$ , and the first term on the right side of Equation 35 is generated by  $V_{-1,\text{LR}}^{\text{PV}}$  as computed by Desplanques & Benayoun using the Reid Soft Core potential (92). Because  $V_{1,\text{MR}}^{\text{PV}}$  contains spin-isospin structures corresponding to both the  $C_6$  and  $C_2$  terms in  $V_{1,\text{SR}}^{\text{PV}}$ , the LEC  $\lambda_s^1$  will also contain a dependence on  $h_\pi^1$  generated by two-pion exchange. In addition to computing these new

contributions to  $\rho_t$  and  $\lambda_s^1$ , theorists must also determine new meson-exchange current contributions to processes such as  $\bar{n} + p \rightarrow d + \gamma$ , associated with  $V_{1,MR}^{PV}$  and  $V_{1,LR}^{PV}$  and required by gauge invariance, as well as the contribution from the new current in Equation 29.

Assuming that a successful program is completed and the complete set of PV LECs through  $\mathcal{O}(Q)$  are extracted from experiment, the values of these parameters would then provide model-independent benchmarks for SM theory. In this case, the theoretical challenge is analogous to the one encountered with  $\chi$ PT for pseudoscalar mesons in which, for example, at  $\mathcal{O}(Q^4)$  there exist 10 independent LECs that have been determined from experiment. The theoretical task now is to explain how the dynamics of QCD give rise to the values of these constants, and to that end a number of approaches have been pursued. Ultimately, of course, one would prefer to compute these constants using lattice QCD, but given the difficulties in putting two or more hadrons on the lattice, approaches based on symmetry arguments or models are an attractive interim alternative. A particularly fruitful direction involves taking the limit of QCD with a large number of colors ( $N_C$ ), wherein the exchange of heavy mesons, such as the  $\rho$  and  $\omega$ , are expected to dominate the underlying QCD dynamics of the LECs. In the  $N_C = 3$  world that we inhabit, this large- $N_C$  picture of resonance saturation works remarkably well in accounting for the values of the constants. It remains to be understood why the large- $N_C$  limit is so successful in this case, and future lattice QCD computations should address this problem.<sup>9</sup>

In the case of the PV LECs, the results from experiment should teach us whether the large- $N_C$  resonance saturation picture applies to the  $\Delta S = 0$  HWI involving baryons as well as to strong interactions between light mesons. In effect, the DDH model assumes the validity of resonance saturation, albeit with a truncated spectrum of exchanged mesons that may or may not reflect accurately the underlying dynamics. As discussed above, ample evidence exists that QCD symmetry arguments fall short when confronting the phenomenology of the  $\Delta S = 1$  HWI, so one should apply caution when adopting another one (viz, large  $N_C$ ) to predict weak, hadronic  $\Delta S = 0$  processes. However, the goal is to derive as much model-independent information as possible on the HWI in each sector so that new insights can be gained into the puzzles associated with strangeness-changing processes. For example, should a set of experimentally determined PV LECs agree with expectations based on NDA and resonance saturation, one might conclude that the breakdown of symmetry-based expectations in the  $\Delta S = 1$  sector is associated with the dynamics of the participating strange quark. Alternatively, should the PV LECs depart substantially from NDA and large- $N_C$

---

<sup>9</sup>It has also become important to know the values of certain  $\mathcal{O}(Q^6)$  constants that presently cannot be taken from experiment and that are needed for the extraction of the Cabibbo-Kobayashi-Maskawa matrix element  $V_{us}$  from  $K_{e3}$  decay data. The insights and techniques developed to explain the  $\mathcal{O}(Q^4)$  constants will be essential in obtaining reliable theoretical values for the unknown higher-order terms.

expectations, one would look elsewhere to determine dynamics general to all sectors of the HWI.

### 3.3. Recent Theoretical Work

As the foregoing discussion makes evident, there now exists ample motivation for new theoretical work within the context of the EFT for hadronic PV. The past decade has seen initial efforts in this direction, and we review some of this work here.

**3.3.1. FEW-BODY SYSTEMS** In the two-body sector, recent interest has focused on the asymmetry  $A_\gamma^d$  for  $\vec{n}\vec{p} \rightarrow d\gamma$ , where new computations using EFT and Green's function Monte Carlo methods have been used. The lowest-order EFT computation yields the asymmetry (107)

$$A_\gamma^d = -\frac{2m_N}{\gamma^2} \frac{\text{Re}[(X + Y)^*W]}{2|X|^2 + |Y|^2}, \quad 36.$$

where  $X$  and  $Y$  give contributions to the parity-conserving  $\vec{n}\vec{p} \rightarrow d\gamma$  amplitude for an initial  $^3S_1$  and  $^1S_0$  state, respectively, and  $W$  gives the PV amplitude

$$W = -g_A h_\pi^1 \frac{\sqrt{\pi}\gamma}{2\pi F_\pi} \left[ \frac{m_\pi}{(m_\pi + \gamma)^2} - \frac{m_\pi^2}{2\gamma^3} \ln\left(\frac{2\gamma}{m_\pi} + 1\right) + \frac{m_\pi^2}{\gamma^2(m_\pi + \gamma)} \right], \quad 37.$$

where  $\gamma = \sqrt{m_N B}$  and  $B$  is the deuteron binding energy.<sup>10</sup> From these expressions,  $A_\gamma^d = -0.17h_\pi^1$ . The coefficient of  $h_\pi^1$  in this result is nearly a factor of two larger than in previous wavefunction-based computations and has stimulated considerable follow-up theoretical activity (41, 42, 66, 108, 110). In particular, the authors of Reference 110 computed the asymmetry to NLO in the Weinberg scheme using two-body wavefunctions derived from the Argonne  $v_{18}$  potential and obtained  $A_\gamma^d = -0.10h_\pi^1$ , a value in close agreement with previous results obtained using Siegert's theorem,  $A_\gamma^d \simeq -0.11h_\pi^1$ . Subsequently, the authors of Reference 41 performed a wavefunction-based computation in the DDH framework using Argonne  $v_{18}$ , Nijmegen-I, and Bonn-CD wavefunctions and found  $A_\gamma^d = -(0.106 \rightarrow 0.109)h_\pi^1 + \dots$ , where the range corresponds to the choice of different potentials and where  $+\dots$  indicates small  $\mathcal{O}(10^{-9})$  contributions from the short-range terms in the DDH potential.

From a more academic perspective, several computations of the deuteron anapole moment have been performed using EFT and wavefunction methods (67, 111–114). The LO EFT result is (111)

$$F_A^{(D)} = -\frac{eg_A h_\pi^1 m_N^2}{24F_\pi} \left[ \kappa_1 \frac{m_\pi + \gamma}{(m_\pi + 2\gamma)^2} + \frac{2m_\pi + 9\gamma}{6(m_\pi + 2\gamma)^2} \right], \quad 38.$$

<sup>10</sup>In Equation 37 we used an overall sign that is opposite the one appearing in Reference 107, thereby following the conventions used elsewhere in the literature (108, 109).

where  $\kappa_1 \simeq 1.85$  is the isovector anomalous magnetic moment of the deuteron. The numerical value of  $F_A^{(D)}$  obtained from this expression has the same sign but a magnitude that is  $\sim 40\text{--}50\%$  larger than results obtained using a wavefunction computation (67) or Weinberg EFT approach (113). From a practical standpoint, the impact of the deuteron anomalous moment is most relevant to the interpretation of PV elastic  $\vec{e}d$  scattering, wherein it would generate a potentially important contribution to the isoscalar axial vector response (35). Because the latter vanishes at tree level in the SM, it is particularly transparent to higher-order effects, such as electroweak radiative corrections, the strange quark axial vector current, and hadronic PV. To date, however, no experiments have been proposed to study the PV elastic deuterium asymmetry.

**3.3.2. SINGLE-NUCLEON SECTOR** From the standpoint of theoretical interpretability, PV pion photo- and electroproduction processes involving single-nucleon targets offer several advantages. In particular, they provide a means for directly accessing the PV  $\pi NN$  couplings without having to disentangle the short- and medium-range effects discussed above. Moreover, the use of  $\chi$ PT to describe low-energy pion-nucleon interactions is well established and has been thoroughly studied in the parity-conserving sector. Looking to future work in QCD, it is likely that attempts to compute the PV  $\pi NN$  couplings on the lattice will precede any efforts to study the short-range PV interaction.

Two decades ago Woloshyn (115) and Li et al. (116) studied single-nucleon, PV pion photo- and electroproduction processes in the meson-exchange framework. These authors found that PV asymmetries for the scattering of longitudinally polarized photons should be of order a few  $\times 10^{-7}$ , assuming the DDH best value for  $h_\pi^1$ , whereas those for electroproduction could be up to two orders of magnitude larger. Given the experimental challenges associated with such tiny asymmetries, and the prospect of measuring considerably larger effects in light nuclei, the prospects for carrying out single-nucleon studies were largely ignored for many years.

Recently, however, advances in experimental techniques for measuring  $\mathcal{O}(10^{-7})$  photo- and electroproduction asymmetries have stimulated renewed interest in this direction. Theoretically, Chen & Ji reformulated the earlier work for near-threshold PV pion photo- (117) and electroproduction (118) using heavy baryon  $\chi$ PT. Subleading contributions were subsequently considered by the authors of Reference 119. To  $\mathcal{O}(Q)$ , the threshold photoproduction asymmetry is

$$B_\gamma = \frac{\sqrt{2}F_\pi}{g_A m_N} \left[ \mu_p - \mu_n \left( 1 + \frac{m_\pi}{m_N} \right) \right] h_\pi^1 + \frac{4\sqrt{2}m_\pi}{g_A \Lambda_\chi} \bar{C}_\pi, \quad 39.$$

where  $\Lambda_\chi = 4\pi F_\pi$  and the terms proportional to  $m_\pi$  give the  $\mathcal{O}(Q)$  contributions. A measurement at Jefferson Laboratory could in principle yield a result for  $B_\gamma$  with statistical accuracy at better than the  $10^{-7}$  level; however, substantial technical challenges associated with the implied current-mode pion detection would have to be overcome to design a successful experiment.

Considerably larger photo- and electroproduction asymmetries may be observed in the vicinity of the  $\Delta(1232)$  resonance. The asymmetry in this region is dominated by the lowest-order PV  $\gamma N \Delta$  interaction that does not contribute strongly at lower energies (120):

$$\mathcal{L}_{\text{PV}}^{\Delta N \gamma} = i \frac{e}{\Lambda_\chi} [d_\Delta^+ \bar{\Delta}_\mu^+ \gamma_\lambda p + d_\Delta^- \bar{\Delta}_\mu^0 \gamma_\lambda n] F^{\mu\lambda} + \text{h.c.}, \quad 40.$$

where the  $d_\Delta^\pm$  are LECs that govern the strength of the PV transition. For  $E_\gamma \approx m_\Delta - m_N$ , the PV photoproduction asymmetry is

$$B_\gamma^\pm \approx -\frac{2d_\Delta^\pm m_N}{C_3^V \Lambda_\chi} + \dots, \quad 41.$$

where  $C_3^V \sim 2$  is the transition magnetic moment and  $+\dots$  indicates higher-order, chiral corrections. The latter have been computed in Reference 121 and were shown to be relatively small. Thus, the size of the resonance asymmetry is essentially set by  $d_\Delta^\pm$ .

The authors of Reference 121 noted that a determination of  $d_\Delta^\pm$  could provide additional insights into the puzzles surrounding the  $\Delta S = 1$  HWI discussed above. In particular, if the dynamics responsible for the enhanced PV hyperon radiative decay asymmetries also occur for the  $\Delta S = 0$  PV  $N \rightarrow \Delta$  transition,  $B_\gamma^\pm$  could be as large as a few  $\times 10^{-6}$ . Such an effect could be observed in forward-angle PV electroproduction experiments, for which the contribution of  $Z^0$  exchange becomes kinematically suppressed, thereby exposing the  $d_\Delta$  contribution (121). However, if the occurrence of enhanced PV asymmetries is unique to the  $\Delta S = 1$  sector and is associated with the presence of valence strange quarks, then  $B_\gamma^\pm$  is likely to be smaller by an order of magnitude or more.

With this motivation in mind, possibilities for measuring  $B_\gamma^\pm$  using both the G0 and  $Q_{\text{weak}}$  instrumentation at Jefferson Laboratory are being actively pursued. The G0 collaboration will measure inclusive pion asymmetries in an upcoming backward-angle run on a deuterium target (122). A measurement of the PV asymmetry in inclusive inelastic  $ep$  scattering at much lower  $Q^2$  to  $\simeq 0.09$  ppm is also envisioned as a future enhancement of the  $Q_{\text{weak}}$  experimental program (123).

An alternative to photo- and electroproduction is PV Compton scattering from the nucleon. Computations of the asymmetry for scattering with either polarized protons or polarized photons have been carried out in References 124 and 125. The asymmetry in both cases is proportional to  $h_\pi^1$  at LO. For  $E_\gamma \ll m_\pi$  and center-of-mass scattering angle  $\theta = \pi/2$  (125),

$$A_{\bar{\gamma}p \rightarrow \gamma p} \sim 8.8 \times 10^{-9} \left( \frac{h_\pi^1}{5 \times 10^{-7}} \right) \left( \frac{E_\gamma}{70 \text{ MeV}} \right)^3, \quad 42.$$

where higher-order corrections are expected to yield corrections of order 25% and  $h_\pi^1$  has been scaled to the magnitude expected from NDA. Thus, an asymmetry of order a few  $\times 10^{-8}$  is expected—roughly the size of the asymmetry expected

in  $\bar{n} + p \rightarrow d + \gamma$ . The magnitude of the Compton scattering asymmetry with a polarized target is similar. To date, no experimental proposals have been developed for measuring either asymmetry.

**3.3.3. COMPUTING  $h_\pi^1$  IN QUANTUM CHROMODYNAMICS** Much of the recent theoretical focus has fallen on extracting the leading PV pion-nucleon coupling in a way that does not require knowledge of the other PV LECs or of many-body nuclear physics. The interest in  $h_\pi^1$  has also stimulated new analyses of QCD predictions for this quantity that attempt to go beyond the work of DDH. A first-principles computation will ultimately require use of lattice QCD, and although we are not aware of immediate plans to carry out such a calculation, some of the necessary theoretical groundwork has recently been laid. In particular, tractable lattice computations typically involve use of quarks that are heavier than the physical light quarks, so to obtain a physically realistic QCD prediction from a lattice result, the quark mass dependence of a given quantity needs to be known.<sup>11</sup> To that end,  $\chi$ PT provides the necessary link because the chiral expansion in powers of  $m_\pi$  is equivalent to an expansion in  $\sqrt{m_q}$ .

The first such analysis of  $h_\pi^1$  was performed by Zhu et al. (126), who employed  $SU(2)_L \times SU(2)_R$   $\chi$ PT with explicit  $\Delta$  isobar degrees of freedom and computed all contributions to  $\mathcal{O}(Q^3)$ . These contributions arise from one-loop diagrams of the type illustrated in Figure 11. Naively, one expects the loop contributions to be suppressed by powers of  $(Q/\Lambda_\chi)^k$  for  $k = 2, 3$ , where  $\Lambda_\chi = 4\pi F_\pi \sim 1$  GeV and  $Q$  is either  $m_\pi$  or  $m_\Delta - m_N$ . In the case of  $h_\pi^1$ , however, the one-loop contributions receive logarithmic and fortuitous numerical enhancements, leading to the renormalized coupling

$$h_\pi^1 = 0.5\mathring{h}_\pi^1 + 0.25h_A^1 - 0.24h_\Delta + 0.08h_A^\Delta, \quad 43.$$

where  $\mathring{h}_\pi^1$  is the bare  $\pi$ NN PV Yukawa coupling,  $h_\Delta$  is the analogous PV  $\pi N \Delta$  Yukawa coupling,  $h_A^1$  parameterizes the isovector  $\pi$ NN PV derivative coupling

$$\mathcal{L}_A^{\pi NN} = i \frac{h_A^1}{F_\pi^2} \bar{N} \gamma^\mu \gamma_5 N (\pi^+ D_\mu \pi^- - \pi^- D_\mu \pi^+) + \dots, \quad 44.$$

and  $h_A^\Delta$  parameterizes analogous PV  $\pi N \Delta$  derivative couplings.

The corrections appearing in Equation 43 are only those having nonanalytic quark mass dependence  $m_q \ln m_q$  or  $m_q^{3/2}$  (in the  $m_\Delta = m_N$  limit) and are uniquely identified with chiral loops.<sup>12</sup> As discussed in Reference 126, terms of this form cannot arise in quark model matrix elements of the hadronic weak Hamiltonian that were used in the analysis of DDH. Moreover, the sum rule contribution to  $h_\pi^1$  that DDH derived from  $\Delta S = 1$  decays using  $SU(6)_w$  symmetry relied on tree-level

<sup>11</sup>The advent of chiral quarks has reduced the range over which an extrapolation must be performed.

<sup>12</sup>Terms that are analytic in  $m_q$  can be absorbed into corresponding terms in the Lagrangian.

symmetry relations that do not contain  $m_q$ -dependent symmetry-breaking effects generated by chiral loops. Thus, it appears unlikely that DDH benchmark estimates for  $h_\pi^1$  fully reflect the impact of its quark mass dependence. Interestingly, the magnitudes of the coefficients of the various terms in Equation 43 are comparable, allowing for possible cancellations between them, which could reduce the magnitude of  $h_\pi^1$  from the DDH “best value.” In principle, a study of  $h_\pi^1$  on the lattice could allow one to identify the unknown constants appearing in Equation 34 by varying both  $m_q$  and the number of colors.

At present, carrying out such an analysis with unquenched QCD is prohibitively expensive. An alternative approach, which allows one to extrapolate lattice computations to the domain of the physical, light quarks, involves varying the valence and sea quark masses independently, a technique known as partial quenching. To identify the  $m_q^{\text{valence}}$  and  $m_q^{\text{sea}}$  dependence analytically from one-loop computations, standard  $\chi$ PT must be generalized to the corresponding partially quenched effective theory (127). A computation using this framework has been performed in Reference 128, leading to an expression analogous to that of Equation 43, which gives the nonanalytic valence and sea quark mass dependence in the partially quenched theory. An extrapolation to the chiral domain also requires inclusion of analytic terms that can be obtained from the effective Lagrangian and that were not written down explicitly in Reference 128.

As of this writing, the first-principles QCD analysis of  $h_\pi^1$  has not advanced beyond the analytic work of References 126 and 128. Given the new experimental efforts, the time is clearly right for an investment in a lattice computation of  $h_\pi^1$ . On a longer-term horizon, one would also hope to see lattice predictions of the constants  $C_i$  and  $\tilde{C}_i$ , which parameterize the  $\mathcal{O}(Q)$  short-distance, PV four-nucleon operators discussed above. Obtaining such computations likely depends on progress in lattice calculations of the low-energy, strong NN interaction. Savage and collaborators are carrying out a program aimed in this direction (M.J. Savage, private communication).

In the absence of first-principles QCD computations of the PV constants, nucleon model calculations may provide an indication of their magnitudes. The expectations derived from the DDH  $SU(6)_w$ /quark model treatment (6) has been discussed above. Alternate approaches have recently been used to predict  $h_\pi^1$ . In the three-flavor Skyrme model of Reference 129, the dominant contribution arises from terms in the  $\Delta S = 0$ , PV four-quark Hamiltonian that contain strange quark bilinears such as  $\bar{s}\gamma^\mu s \bar{u}\gamma_\mu \gamma_5 u$ . These terms sample the kaon cloud that arises from the Wess-Zumino action via rotations of the chiral soliton in  $SU(3)$  space. The resulting prediction is  $2g_\pi \lesssim h_\pi^1 \lesssim 3.4g_\pi$ . The corresponding prediction in the two-flavor Skyrme model is considerably smaller. A prediction for a somewhat larger value has been obtained using QCD sum rules (130), wherein one expands nucleon correlators in a pion background in terms of various quark and gluon condensates. Values for the latter, such as  $\langle \bar{q}^i \tau^a \gamma_5 q \rangle_\pi$ , are taken from other nucleon properties, such as the strong  $\pi$  NN coupling, leading to  $h_\pi^1 \sim 8g_\pi$ . Both sets of model predictions are roughly consistent with expectations based on NDA, as

well as the updated “best values” obtained from the  $SU(6)_w$ /quark model approach (6, 13).

### 3.4. Experimental Prospects

In the preceding sections, we emphasized the need for a complete set of precise PV measurements that can be cleanly interpreted in terms of constraints on PV LECs in the NN and few-nucleon systems. As summarized in Table 3, we currently have two significant measurements carried out with low-energy proton beams ( $A_z^{pp}$  and  $A_z^{p\alpha}$ ), and two underway at existing neutron facilities ( $A_\gamma^d$  and  $d\phi^{n\alpha}/dz$ ). As noted above, there is also an existing  $pd$  asymmetry measurement (95) that poses additional theoretical challenges in accounting for the angular dependence in both elastic scattering and breakup channels, which remains to be analyzed in a common framework.

Some immediate prospects for improvement in neutron beam measurements will take advantage of the superior features of a high-intensity pulsed beam facility, the SNS, currently under construction at Oak Ridge, Tennessee. The SNS is anticipated to provide the world’s most intense beams of cold pulsed neutrons, approaching or even surpassing the time-averaged intensities of cw reactor sources (131) by 2008. A crucial advantage of pulsed beams over reactor sources for precision PV experiments results from the introduction of new diagnostic capabilities via time-of-flight analysis of the neutron energy—especially important for reducing  $\gamma$ -ray backgrounds and systematic error diagnosis, as well as neutron polarization diagnostics. In addition, the construction of a new facility allows for the incorporation of technological advances in neutron-guide instrumentation, particularly the use of high-efficiency bent supermirror transport guides, which eliminate direct line of sight between the apparatus and the cold moderator, thereby reducing  $\gamma$ -ray and neutron backgrounds without significant loss of beam flux. The SNS is building a new dedicated beamline, FNPB (131, 132), which is optimized to the needs of a suite of precision experiments in HWI and neutron  $\beta$ -decay.

**3.4.1. NEUTRON CAPTURE GAMMA-ASYMMETRY MEASUREMENTS** As discussed above, the LANSCE phase of the ongoing NPDGamma experiment to measure  $A_\gamma^d$  will be statistics limited at the  $10^{-7}$  level, whereas the expected asymmetry based on the NDA and DDH “best value” estimates for  $h_\pi^1$  is  $A_\gamma^d = -5 \times 10^{-8}$ . NPDGamma is expected to be a key element of the initial SNS fundamental neutron physics program (133). At the time of writing, the apparatus has been commissioned, and systematic errors have been extensively studied at LANSCE, where the apparatus is awaiting installation of the liquid parahydrogen target in 2006. A conclusion of these studies is that the apparatus is ready to make a measurement of  $A_\gamma^d$  with a statistical error of  $1 \times 10^{-8}$ . Systematic errors are expected to be at or below the  $10^{-9}$  level; however, additional running time to measure the potential false asymmetry from aluminum vacuum windows is needed to reach the ultimate experimental precision that can be achieved at the SNS.

The SNS FNPB beamline has been extensively studied via Monte Carlo simulations, and reasonably conservative flux estimates indicate that a measurement of  $A_\gamma^d$  at the  $1 \times 10^{-8}$  level should be possible in approximately 5000 hours of running on the new beamline once the SNS reaches 1.4 MW operation. The experiment can be moved with only minimal changes required to the apparatus because the beam conditions (apart from increased flux) will be quite similar to those at LANSCE. The NPDGamma apparatus will be used to commission the new FNPB beamline when it comes on line, anticipated in 2008. In addition to the higher beam flux, two significant improvements in experimental conditions that could further improve the experimental precision are anticipated at the SNS. Gamma background reduction will be achieved in part as a result of the SNS curved neutron guide and in part with the incorporation of additional lead shielding upstream of the main detector array. Higher beam polarization should also be possible via a combination of increased laser pumping power and the use of spectrally narrowed lasers for optical pumping of the  $^3\text{He}$  spin filter cell, which produces up to 75% polarization in bench tests as compared with the 40–55%  $^3\text{He}$  polarization routinely achieved during extended running in Flight Path 12 at LANSCE (133).

As noted above, the PV gamma asymmetry  $A_\gamma^t$  in the reaction  $\bar{n} + d \rightarrow t + \gamma$  provides a complementary window on the  $\Delta S = 0$  HWI to its counterpart in the  $np$  system. A Letter of Intent has been submitted to the SNS to develop this experiment as a logical follow-up to the NPDGamma experiment (134). As indicated in Table 3,  $A_\gamma^t$  displays a much larger sensitivity to the PV LECs, including a  $\sim 30$  times stronger sensitivity to  $h_\pi^1$ , than does  $A_\gamma^d$ . On the basis of the various estimates for the PV LECs (Table 2),  $A_\gamma^t$  could be as much as one to two orders of magnitude larger than  $A_\gamma^d$ .

In principle, the  $nd$  asymmetry measurement can be performed using most of the components of the NPDGamma apparatus, with an obvious exception of the target. The experiment is technically much more challenging than the  $np$  case because of the much smaller  $nd$  capture cross section; consequently, most of the neutrons will scatter out of the target rather than be captured to produce the  $\gamma$  rays of interest. A room temperature liquid  $\text{D}_2\text{O}$  target is under consideration, with a length optimized between two competing factors—the very small  $nd$  capture cross section and the desire to avoid significant neutron depolarization in the target. A novel target vessel and shielding scheme are required to absorb the scattered neutrons without producing significant background  $\gamma$  rays. The interactions of polarized cold neutrons in  $\text{D}_2\text{O}$  are at present not well understood, and a program of detailed simulations and test measurements will be carried out to optimize the design of the experiment. Other target possibilities include cold solid orthodeuterium or solid ortho- $\text{D}_2\text{O}$  in an effort to minimize depolarization by slowing down the neutron beam, thereby increasing the capture probability (W.M. Snow, private communication). An earlier measurement of  $A_\gamma^t$  was carried out at ILL and found a result consistent with zero:  $A_\gamma^t = (4.2 \pm 3.8) \times 10^{-6}$  (135, 136); the goal of the proposed SNS measurement is to reach a sensitivity  $4 \times 10^{-7}$ . Many

of the systematic effects are similar to those for the  $np$  experiment, where they have been extensively studied. It should be noted that the absolute tolerance for systematic errors is relaxed for the  $nd$  experiment because the absolute precision goal is more than an order of magnitude less stringent than that for the  $np$  experiment.

**3.4.2. NEUTRON SPIN ROTATION MEASUREMENTS** As for the neutron capture asymmetry measurements, the higher neutron flux anticipated for the SNS as well as the pulsed nature of the beam offer compelling advantages for improving the precision of the  $n\alpha$  PV spin rotation measurement, as well as the possibility of carrying out experiments on  $np$  and perhaps even  $nd$  spin rotation. To date, a Letter of Intent has been submitted for the  $n\alpha$  experiment (137), anticipating a measurement accuracy of  $1 \times 10^{-7}$  rad/m in 12 months of data taking, which would represent a factor of three improvement over what is currently expected at NIST, with improved systematic error control. It is likely that the  $n\alpha$  spin rotation experiment will run at the SNS quite early in the FNPB experimental program. The collaboration intends in the longer term to pursue  $np$  spin rotation at the SNS as well (138). The sensitivity of the  $n\alpha$  spin rotation experiment to the five PV LECs in the pionless EFT is given in Table 3 (predictions in the DDH meson-exchange model are available for the  $np$  and  $n\alpha$  cases, as mentioned in Section 2.2.3).

The basic spin rotation experimental technique has been outlined in Section 2.2.3; recall the crucial role of the  $\pi$  coil in Figure 10, which is used to suppress the effect of the much larger spin precessions caused by residual magnetic fields inside the apparatus. Because previous experiments have been carried out at reactor facilities with polychromatic cold neutron beams, the best option was to optimize the field in the  $\pi$  coil to rotate the neutron spins on average by  $180^\circ$  between the upstream and downstream segments of the apparatus. Nearly a factor of two improvement can be obtained at a pulsed source (138) by ramping the  $\pi$ -coil current as a function of time of flight to provide a  $180^\circ$  spin rotation for all neutron velocities. In addition, one can take advantage of the fact that the PV spin rotation is independent of neutron velocity, whereas scattering and magnetic field effects are in general energy- and thus velocity-dependent for diagnosis of systematic effects. For the hydrogen and possible deuterium target measurements, neutron depolarization must be avoided by preparing cryogenic liquid targets in spin-selected molecular states—paramolecular for hydrogen and orthomolecular for deuterium—an additional complication, particularly considering the requirement for constant cycling of the liquid between front and rear target locations. For neutron energies below 15 meV, depolarization does not occur in parahydrogen. Less is known about the case for orthodeuterium, but a recent measurement at PSI found negligible depolarization of cold neutrons on orthodeuterium for a 4-cm target (W.M. Snow, private communication), which is encouraging news for the prospect of a deuterium spin rotation measurement.

## 4. BEYOND HADRONIC PARITY VIOLATION

Throughout this review, we have emphasized the significance of hadronic PV as a probe of the strangeness-conserving HWI. Here, we comment briefly on its implications for other processes. We have already encountered one such process—PV electron scattering—discussed in Section 2.1. There, contributions from hadronic PV to the PV asymmetries constitute a theoretical background that must be computed reliably to extract information on other quantities of interest, such as the strange quark form factors.

A second illustration concerns neutrinoless double  $\beta$ -decay ( $0\nu\beta\beta$ ). This process is of considerable current interest, as it provides the only known way to determine whether neutrinos are Majorana fermions (for recent reviews, see e.g., References 139 and 140). In addition, one also hopes to use  $0\nu\beta\beta$  to determine the absolute scale of neutrino mass, complementing what we know about  $m_\nu$  from tritium  $\beta$ -decay and about neutrino mass differences from oscillation studies.

Unfortunately, the latter use of  $0\nu\beta\beta$  is complicated by possible contributions to the rate from the exchange of heavy Majorana particles, such as a heavy Majorana neutrino or the neutralinos of supersymmetry. To determine the absolute scale of  $m_\nu$ , the amplitude  $A_H$  for heavy particle-exchange contributions, which can be comparable in magnitude to the amplitude  $A_L$  for light Majorana neutrino exchange, must be known. From simple dimensional arguments (141),

$$\frac{A_H}{A_L} \sim \frac{M_W^4 \bar{k}^2}{\Lambda^5 m_{\beta\beta}}, \quad 45.$$

where  $m_{\beta\beta}$  is the effective mass of the light Majorana neutrino having typical virtuality  $\bar{k}^2 \sim (50 \text{ MeV})^2$  and  $\Lambda$  is the mass scale associated with the heavy Majorana particles. Given what we know about  $\Delta m_\nu^2$  and the neutrino-mixing matrix elements that help determine  $m_{\beta\beta}$ , the ratio in Equation 45 can be  $\mathcal{O}(1)$  for  $\Lambda$  of order 1 TeV. Thus, it is important to analyze the possible heavy particle contributions with theoretical clarity.

Recently, an EFT approach for doing so was developed by the authors of Reference 142. At the lepton-quark level, the effective operators for heavy Majorana particle exchange factorize into products of four-quark and two-lepton operators. The four-quark operators are analogous to those entering the  $\Delta S = 0$  HWI, differing only in their respective representations in chiral SU(2). Consequently, the mapping of these operators onto effective hadronic operators involving nucleon and pion degrees of freedom is similar to the one used in obtaining the EFT for hadronic PV. Thus, the study of hadronic PV should provide insights into the EFT for heavy particle contributions in  $0\nu\beta\beta$ . We consider two aspects of this correspondence in particular:

1. In contrast to the situation for hadronic PV, there is no program of few-body experiments from which one can determine the operator coefficients for the

$0\nu\beta\beta$  EFT. These coefficients must be computed theoretically. Comparisons of analogous computations of the LECs for hadronic PV with experimental values should provide new guidance for obtaining reliable computations in the  $0\nu\beta\beta$  case. Indeed, as argued above, hadronic PV provides a unique tool for learning how the strong interaction dresses four-quark weak interactions into hadronic operators and amplitudes.

2. Again in contrast to hadronic PV,  $0\nu\beta\beta$  can occur only in heavy, complex nuclei. Although there has been considerable recent progress in understanding how an EFT power counting of operators translates into a power counting of few-body matrix elements, the situation with complex nuclei is less clear. For the EFT to provide realistic guidance to the size of heavy particle contributions to  $0\nu\beta\beta$  transition matrix elements, we need to know how well operator power counting works for nuclear matrix elements.

In principle, hadronic PV can provide useful insights into this issue. Because the lowest-order PV interaction can be determined from a program of few-body experiments as outlined above, this interaction can then be used as a known probe of nuclear PV observables, such as the nuclear anapole moment or the PV  $\gamma$ -decays of p-shell nuclei. To the extent that the lowest-order PV interaction suffices to yield successful descriptions of these nuclear PV observables, there would be evidence for the applicability of the EFT to nuclei. To the extent that it does not, many-body renormalization of the lowest-order weak effective interaction would likely be substantial and high-momentum components of nuclear wavefunctions would likely play a more important role than one might naively expect. Either way, the implications for  $0\nu\beta\beta$  would be important.

## 5. SUMMARY AND CONCLUSIONS

The quest to explain the manifestations of weak interactions between quarks in strongly interacting systems remains an important piece of unfinished business for SM physics. In both the  $\Delta S = 1$  and  $\Delta S = 0$  sectors, the nonperturbative character of low-energy QCD has been the stumbling block. The  $\Delta S = 1$  decays of hyperons in particular seem to elude explanation using the standard symmetry and EFT approaches that have been so successful in treating low-energy strong interactions. Whether these puzzles simply reflect the active participation of the strange quark with its mass of order the QCD scale, or some other dynamics peculiar to HWIs, is unknown. Our hope is that through experimental studies of the  $\Delta S = 0$  HWI with PV observables and through their theoretical interpretation within the EFT framework that makes for the closest possible contact with QCD, we will gain new insights into the low-energy weak interactions of the three lightest quarks. We hope to have sketched a useful roadmap for future progress in this direction.

As we have emphasized throughout, the forefront in this endeavor lies in the arena of single-nucleon and few-body nuclear systems. Experimental developments have paved the way for completion of precise measurements of the  $\mathcal{O}(10^{-7})$

PV effects in such systems, and plans are underway for several new few-body experiments. The immediate theoretical challenge is to compute the few-body PV observables using the EFT framework, allowing one to extract robust values for the LECs from experiment. In the long term, we would like to determine the extent to which these results are consistent with SM-based expectations, both from the standpoint of symmetries and from first-principles lattice calculations. In light of the substantial experimental and theoretical progress in the field as well as the significant new opportunities made possible by this progress, we are optimistic that this effort can be successful.

## ACKNOWLEDGMENTS

The authors would like to thank S. Ando, J. Carlson, B. Desplanques, M.T. Gericke, G. Gwinner, G.L. Greene, W.C. Haxton, B.R. Holstein, C.-P. Liu, C. Maekawa, W.M. Snow, U. van Kolck, and S.-L. Zhu for helpful discussions. This work was supported in part under Department of Energy contract FG02-05ER41361, National Science Foundation Award PHY-0071856, and by grants from the Natural Sciences and Engineering Research Council (Canada) and the National Science Foundation.

**The Annual Review of Nuclear and Particle Science is online at  
<http://nucl.annualreviews.org>**

## LITERATURE CITED

1. Tanner N. *Phys. Rev.* 107:1203 (1957)
2. Feynman R, Gell-Mann M. *Phys. Rev.* 109:193 (1958)
3. Lobashov VM, et al. *Sov. Phys. J. Exp. Theor. Phys.* 5:59 (1967)
4. Lobashov VM, et al. *Phys. Lett. B* 25:104 (1967)
5. Bowman CD, Bowman JD, Yuan VW. *Phys. Rev. C* 39:1721 (1989)
6. Desplanques B, Donoghue JF, Holstein BR. *Ann. Phys.* 124:449 (1980)
7. Haxton WC, Liu CP, Ramsey-Musolf MJ. *Phys. Rev. C* 65:045502 (2002)
8. Zhu SL, et al. *Nucl. Phys. A* 748:435 (2005)
9. Adelberger EG, Haxton WC. *Annu. Rev. Nucl. Part. Sci.* 35:501 (1985)
10. Desplanques B. *Phys. Rep.* 297:1 (1998)
11. Haeblerli W, Holstein B. In *Symmetries and Fundamental Interactions in Nuclei*, pp. 17–66. Singapore: World Sci. (1995)
12. Dubovik VM, Zenkin SV. *Ann. Phys.* 172:100 (1986)
13. Feldman GB, Crawford GA, Dubach J, Holstein BR. *Phys. Rev. C* 43:863 (1991)
14. Barton G. *Nuovo Cim.* 19:512 (1961)
15. Holstein BR. *Phys. Rev. D* 23:1618 (1981)
16. Zeldovich Y. *Sov. Phys. J. Exp. Theor. Phys.* 6:1184 (1958)
17. Musolf MJ, Holstein BR. *Phys. Rev. D* 43:2956 (1991)
18. Flambaum VV, Khriplovich IB. *Sov. Phys. J. Exp. Theor. Phys.* 52:835 (1980)
19. Flambaum VV, Khriplovich IB, Sushkov OP. *Sov. Phys. JETP* 60:873 (1984)
20. Haxton WC, Wieman CE. *Annu. Rev. Nucl. Part. Sci.* 51:261 (2001)
21. Dmitriev VF, Khriplovich IB. *Phys. Rep.* 391:243 (2004)
22. Ginges JSM, Flambaum VV. *Phys. Rep.* 397:63 (2004)

23. Haxton WC, Henley EM, Musolf MJ. *Phys. Rev. Lett.* 63:949 (1989)
24. Haxton WC, Liu CP, Ramsey-Musolf MJ. *Phys. Rev. Lett.* 86:5247 (2001)
25. Bouchiat C, Piketty CA. *Z. Phys. C* 49:91 (1991)
26. Bouchiat C, Piketty CA. *Phys. Lett. B* 269:195 (1991)
27. Dmitriev VF, Khriplovich IB, Telitsin VB. *Nucl. Phys. A* 577:691 (1994)
28. Dmitriev VF, Telitsin VB. *Nucl. Phys. A* 674:168 (2000)
29. Wilburn WS, Bowman JD. *Phys. Rev. C* 57:3425 (1998)
30. Auerbach N, Brown BA. *nucl-th/9903032*
31. Bennett LMC, Krien K. *Bull. Am. Phys. Soc.* 25:486 (1980)
32. Haxton WC. *Phys. Rev. Lett.* 46:698 (1981)
33. Musolf MJ, Holstein BR. *Phys. Lett. B* 242:461 (1990)
34. Musolf MJ, Donnelly TW. *Nucl. Phys. A* 546:509 (1992)
35. Musolf MJ, et al. *Phys. Rep.* 239:1 (1994)
36. Hasty R, et al. (SAMPLE Collab.). *Science* 290:2117 (2000)
37. Zhu SL, Puglia SJ, Holstein BR, Ramsey-Musolf MJ. *Phys. Rev. D* 62:033008 (2000)
38. Riska DO. *Nucl. Phys. A* 678:79 (2000)
39. Maekawa CM, van Kolck U. *Phys. Lett. B* 478:73 (2000)
40. Maekawa CM, Veiga JS, van Kolck U. *Phys. Lett. B* 488:167 (2000)
41. Schiavilla R, Carlson J, Paris MW. *Phys. Rev. C* 67:032501 (2003)
42. Liu CP, Prezeau G, Ramsey-Musolf MJ. *Phys. Rev. C* 67:035501 (2003)
43. Ito TM, et al. (SAMPLE Collab.). *Phys. Rev. Lett.* 92:102003 (2004)
44. Spayde DT, et al. (SAMPLE Collab.). *Phys. Lett. B* 583:79 (2004)
45. Holstein BR. *Nucl. Phys. A* 737:85 (2004)
46. Bowman JD, Garvey GT, Johnson MB, Mitchell GE. *Annu. Rev. Nucl. Part. Sci.* 43:829 (1993)
47. Simonius M. *Can. J. Phys.* 66:548 (1988)
48. Berdoz AR, et al. (TRIUMF E497 Collab.). *Phys. Rev. C* 68:034004 (2003)
49. Levy C, et al. *Proc. Workshop Polariz. Ion Sources Polariz. Gas Targets, Madison, Wisconsin, 293:179*. New York: Am. Inst. Phys. (1994)
50. Zelenski AN, et al. *Nucl. Instrum. Methods A* 334:285 (1993)
51. Berdoz AR, et al. *Nucl. Instrum. Methods A* 457:288 (2001)
52. Ramsay W, et al. *Proc. 9th Intl. Workshop Polariz. Sources Targets, Nashville, Indiana*, pp. 289–293. Singapore: World Sci. 289
53. Driscoll DE, Miller GA. *Phys. Rev. C* 40:2159 (1989)
54. Driscoll DE, Miller GA. *Phys. Rev. C* 39:1951 (1989)
55. Iqbal MJ, Niskanen JA. *Phys. Rev. C* 49:355 (1994)
56. Driscoll DE, Meissner UG. *Phys. Rev. C* 41:1303 (1990)
57. Grach I, Shmatikov M. *Phys. Lett. B* 316:467 (1993)
58. Carlson J, Schiavilla R, Brown VR, Gibson BF. *Phys. Rev. C* 65:035502 (2002)
59. Wiringa RB, Stoks VGJ, Schiavilla R. *Phys. Rev. C* 51:38 (1995)
60. Machleidt R. *Phys. Rev. C* 63:024001 (2001)
61. Fujiwara M, Titov AI. *Phys. Rev. C* 69:065503 (2004)
62. Knyazkov V, et al. *Nucl. Phys. A* 417:209 (1984)
63. Earle ED, et al. *Can. J. Phys.* 66:534 (1988)
64. Cavaignac JF, Vignon B, Wilson R. *Phys. Lett. B* 67:148 (1977)
65. Oka T. *Phys. Rev. D* 27:523 (1983)
66. Schiavilla R, Carlson J, Paris MW. *Phys. Rev. C* 70:044007 (2004)
67. Khriplovich IB, Korkin RV. *Nucl. Phys. A* 690:610 (2001)
68. Liu CP, Hyun CH, Desplanques B. *Phys. Rev. C* 69:065502 (2004)
69. Stiliaris E. *Eur. Phys. J.* 24:S2 (2005)

- 
70. Carlson J, Paris M. *Eur. Phys. J. A* 24S1:123 (2005)
  71. Gericke MT, et al. (NPDGamma Collab.) nucl-ex/0507005
  72. Gericke MT, et al. *Nucl. Instrum. Methods A* 540:328 (2005)
  73. Stodolsky L. *Nucl. Phys. B* 197:213 (1982)
  74. Bass C, et al. *J. Res. Natl. Inst. Stand. Technol.* 110:205 (2005)
  75. Markoff D. *Measurement of the parity nonconserving spin-rotation of transmitted cold neutrons through a liquid helium target*. PhD thesis. Univ. Wash., Seattle. 156 pp. (1997)
  76. Dmitriev V, et al. *Phys. Lett.* 125:125 (1983)
  77. Wood CS, et al. *Science* 27:1759 (1997)
  78. Vetter PA, et al. *Phys. Rev. Lett.* 74:2658 (1995)
  79. Guera J, et al. *Phys. Rev. A* 71:042108 (2005)
  80. Dzuba VA, Flambaum VV, Khriplovich IB. *Z. Phys. D* 1:243 (1986)
  81. DeMille D. *Phys. Rev. Lett.* 74:4165 (1995)
  82. Stalnaker J, et al. *Phys. Rev. A* 66: 031403(R)
  83. Gomez E, et al. ph/0412124
  84. Koerber T, et al. *J. Phys. B* 36:637 (2003)
  85. Gomez E, et al. *Rep. Prog. Phys.* 69:79 (2006)
  86. Grossman JS, et al. *Phys. Rev. Lett.* 83:935 (1999)
  87. Gwinner G, et al. *TRIUMF EEC Proposal* E 1065 (2005)
  88. Mitchell GE, et al. *Phys. Rep.* 354:157 (2001)
  89. Tomsovic S, Johnson MB, Hayes A, Bowman JD. *Phys. Rev. C* 62:054607 (2000)
  90. Danilov G. *Phys. Lett.* 18:40 (1965)
  91. Desplanques B, Missimer J. *Nucl. Phys. A* 300:286 (1978)
  92. Desplanques B, Benayoun JJ. *Nucl. Phys. A* 458:689 (1986)
  93. Miller GA. *Phys. Rev. C* 67:042501(2003)
  94. Kloet WM, Gibson BF, Stephenson GJ, Henley EM. *Phys. Rev. C* 27:2529 (1983)
  95. Kistryn S, et al. *Phys. Lett. B* 219:58 (1989)
  96. Fleming S, Mehen T, Stewart IW. *Nucl. Phys. A* 677:313 (2000)
  97. Kaplan DB, Savage MJ, Wise MB. *Phys. Lett. B* 424:390 (1998)
  98. Kaplan DB, Savage MJ, Wise MB. *Nucl. Phys. B* 534:329 (1998)
  99. Weinberg S. *Phys. Lett. B* 251:288 (1990)
  100. Weinberg S. *Nucl. Phys. B* 363:3 (1991)
  101. Beane SR, Bedaque PF, Savage MJ, van Kolck U. *Nucl. Phys. A* 700:377 (2002)
  102. Beane SR, Savage MJ. *Nucl. Phys. A* 713:148 (2003)
  103. Beane SR, Savage MJ. *Nucl. Phys. A* 717:91 (2003)
  104. Kaplan DB, Savage MJ. *Nucl. Phys. A* 556:653 (1993)
  105. Pirner HJ, Riska DO. *Phys. Lett. B* 44:151 (1973)
  106. Manohar A, Georgi H. *Nucl. Phys. B* 234:189 (1984)
  107. Kaplan DB, Savage MJ, Springer RP, Wise MB. *Phys. Lett. B* 449:1 (1999)
  108. Desplanques B. *Phys. Lett. B* 512:305 (2001)
  109. Savage MJ. *Nucl. Phys. A* 695:365 (2001)
  110. Hyun CH, Park TS, Min DP. *Phys. Lett. B* 516:321 (2001)
  111. Savage MJ, Springer RP. *Nucl. Phys. A* 644:235 (1998)
  112. Savage MJ, Springer RP. *Nucl. Phys. A* 686:413 (2001)
  113. Hyun CH, Desplanques B. *Phys. Lett. B* 552:41 (2003)
  114. Liu CP, Hyun CH, Desplanques B. *Phys. Rev. C* 68:045501 (2003)
  115. Woloshyn RM. *Can. J. Phys.* 57:809 (1979)
  116. Li SP, Henley EM, Hwang WYP. *Ann. Phys.* 143:372 (1982)
  117. Chen JW, Ji XD. *Phys. Rev. Lett.* 86:4239 (2001)

118. Chen JW, Ji XD. *Phys. Lett. B* 501:209 (2001)
119. Zhu SL, Puglia S, Holstein BR, Ramsey-Musolf MJ. *Phys. Rev. C* 64:035502 (2001)
120. Zhu SL, Maekawa CM, Holstein BR, Ramsey-Musolf MJ. *Phys. Rev. Lett.* 87:201802 (2001)
121. Zhu SL, et al. *Phys. Rev. D* 65:033001 (2002)
122. Martin J. *Eur. Phys. J. A* 18:425 (2003)
123. Forest TA, et al. *Jefferson Laboratory Letter of Intent*. LOI-03-105 (2003)
124. Bedaque PF, Savage MJ. *Phys. Rev. C* 62:018501 (2000)
125. Chen JW, Cohen TD, Kao CW. *Phys. Rev. C* 64:055206 (2001)
126. Zhu SL, Puglia SJ, Holstein BR, Ramsey-Musolf MJ. *Phys. Rev. D* 63:033006 (2001)
127. Sharpe SR, Shores N. *Phys. Rev. D* 62:094503 (2000)
128. Beane SR, Savage MJ. *Nucl. Phys. B* 636:291 (2002)
129. Meissner UG, Weigel H. *Phys. Lett. B* 447:1 (1999)
130. Henley EM, Hwang WYP, Kisslinger LS. *Phys. Lett. B* 367:21 (1996)
131. Greene GL, et al. *J. Res. Natl. Inst. Stand. Technol.* 110:149 (2005)
132. Huffman P, et al. *J. Res. Natl. Inst. Stand. Technol.* 110:161 (2005)
133. Bowman J, et al. *SNS-FNPF Letter of Intent* (2005)
134. Penttila S, et al. *SNS-FNPF Letter of Intent* (2005)
135. Avenier M, et al. *Nucl. Phys. A* 459:335 (1986)
136. Alberi J, et al. *Can. J. Phys.* 66:542 (1988)
137. Bass C, et al. *SNS-FNPF Letter of Intent* (2005)
138. Markoff DM. *J. Res. Natl. Inst. Stand. Technol.* 110:209 (2005)
139. McKeown RD, Vogel P. *Phys. Rep.* 394:315 (2004)
140. Elliott SR, Engel J. *J. Phys. G* 30:R183 (2004)
141. Cirigliano V, Kurylov A, Ramsey-Musolf MJ, Vogel P. *Phys. Rev. Lett.* 93:231802 (2004)
142. Prezeau G, Ramsey-Musolf M, Vogel P. *Phys. Rev D.* 68:034016 (2003)
143. Eversheim PD, et al. *Phys. Lett. B* 256:11 (1991)
144. Kistryn S, et al. *Phys. Rev. Lett.* 58:1616 (1987)
145. Lang J, et al. *Phys. Rev. Lett.* 54:170 (1985)
146. Alberi J, et al. *Can. J. Phys.* 66:542 (1988)

## NOTE ADDED IN PROOF

After the publication of Reference 8, it was realized that the effects of an additional, long-range PV pion-exchange operator appearing in that work can be absorbed into a combination of one short-range operator and the LO pion-exchange potential (C.-P. & M.J. Ramsey-Musolf, private communication). We thank S. Ando and B. Desplanques for pointing out errors in the corresponding expressions in equation 121 of Reference 8. The corrected formulae appear here.

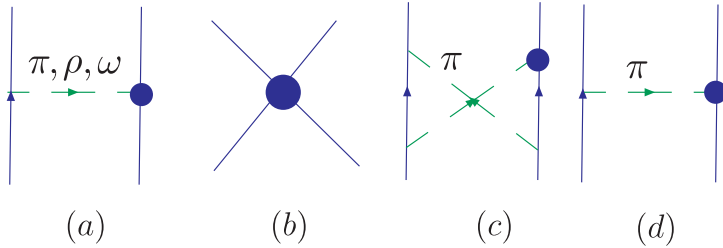


**Figure 1** Comparison of (a) meson-exchange and (b–d) effective field theory treatments of the parity-violating nucleon-nucleon interaction. Panels b, c, and d give illustrative contributions to short-, medium-, and long-range components, respectively.

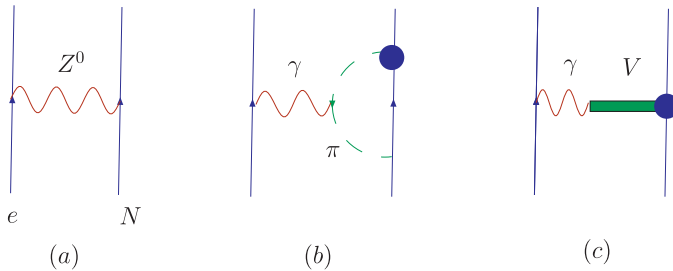


**Figure 3** Contributions from hadronic parity-violating (PV) (proton anapole moment) to the effective axial vector electron-proton coupling,  $G_A^e$ .

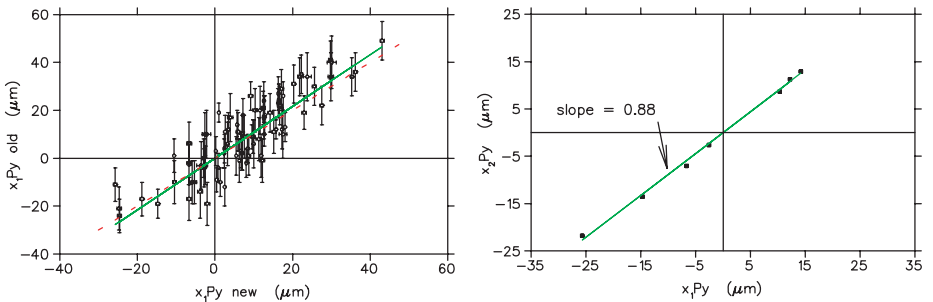


**Figure 5** Demonstration of a new current-mode scanning polarimeter at TRIUMF. (Left panel) Intrinsic polarization moments  $\langle xP_y \rangle$  measured simultaneously with counting-mode (vertical axis) and current-mode (horizontal axis) devices. The errors on the current-mode measurements are too small to display on this scale. The dotted line has a slope of unity, and the solid line is a fit to the data. (Right panel) Intrinsic polarization moments for a given beamline tune, measured with a pair of current-mode polarization profile monitors (PPMs). The ratio of moments at PPM1 and PPM2 remains relatively constant, thus verifying an essential assumption of the systematic error reduction scheme. [Reprinted with permission from Reference 52, Figure 3. Copyright by World Scientific (2002).]

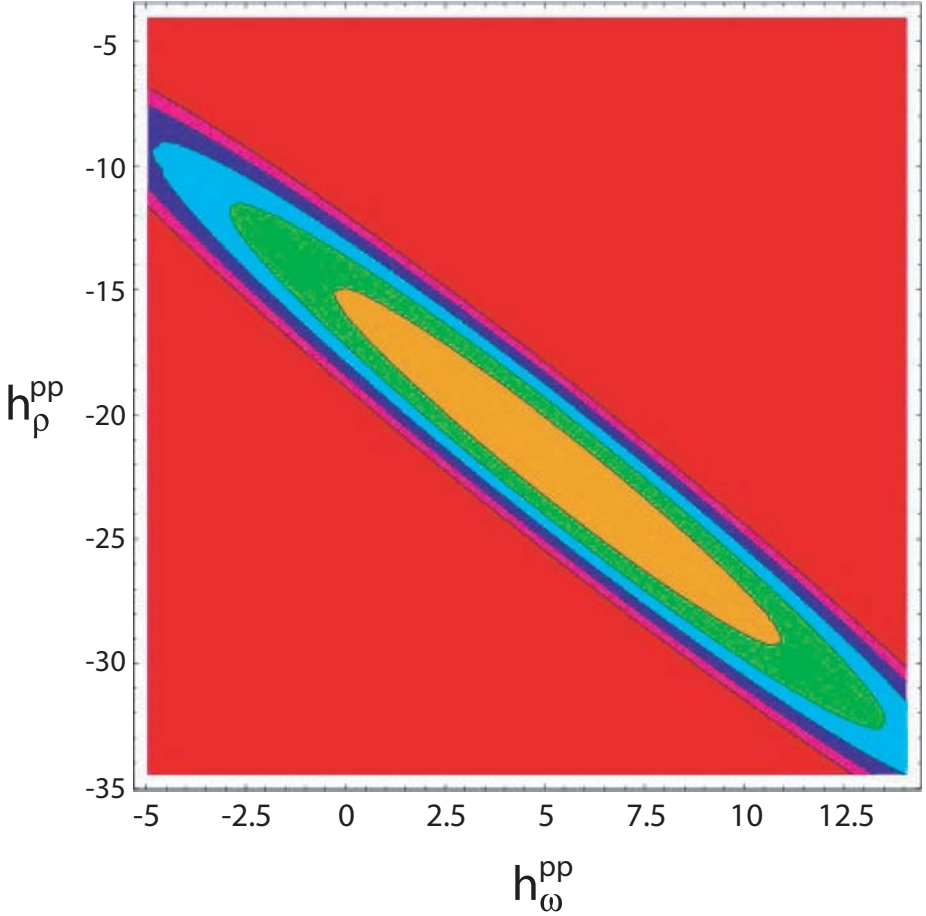


**Figure 7** Present constraints on the weak meson-nucleon couplings  $h_{\rho}^{pp}$  and  $h_{\omega}^{pp}$ , fitted to the low-energy and 221 MeV  $\vec{p}\vec{p}$  asymmetry data (58). The plot shows curves of constant total  $\chi^2 = 1, 2, 3, 4,$  and  $5$ . Axis scales are  $10^{-7}$ . [Reprinted with permission from Reference 58, Figure 8. Copyright by the American Physical Society (2003).]

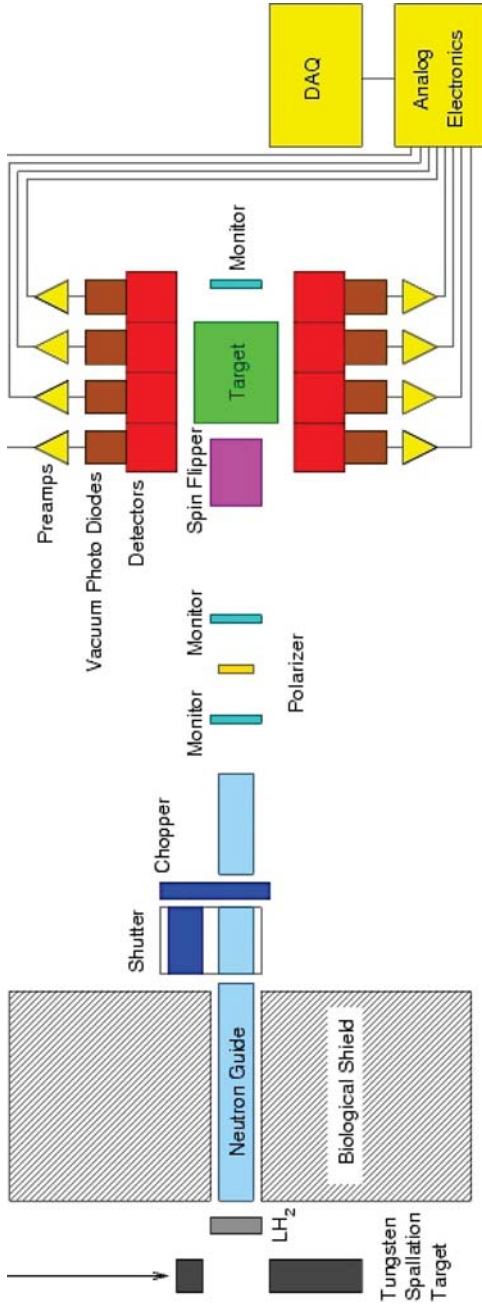


**Figure 8** Layout of the NPDGamma apparatus currently taking data on Flight Path 12 at LANSCE. A set of coils provides a highly uniform, vertical magnetic guide field to preserve the neutron spin direction (not shown).

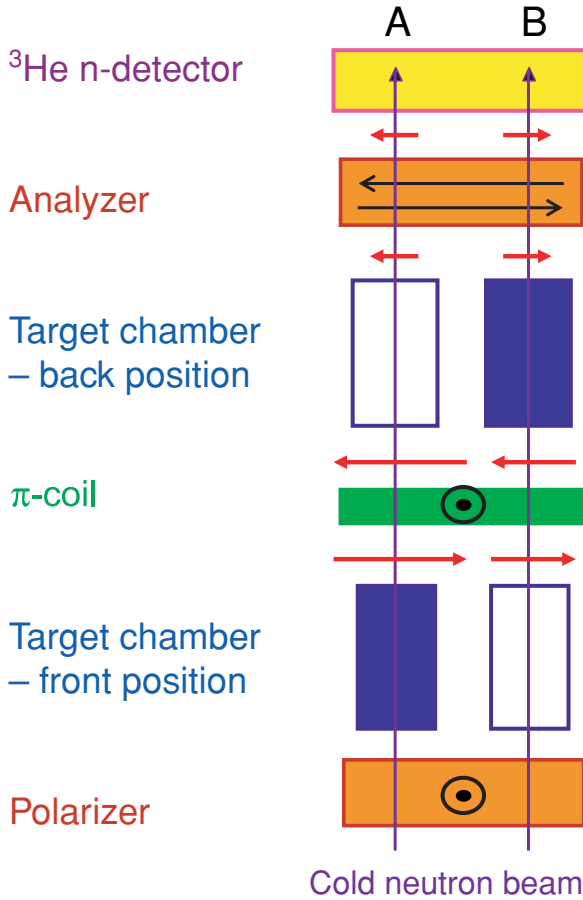


**Figure 10** Schematic of the double beam/double target system for  $^4\text{He}$  neutron spin rotation measurements. The incident neutron spins are polarized out of the page. The parity-violating (PV) effect is a spin precession around the direction of motion, which leads to components in the horizontal plane as shown. The front or back targets are either full or empty in channels A and B. Much larger spin rotations due to local magnetic fields are independent of the target state and are cancelled by subtraction. The  $\pi$  coil situated between the front and rear targets precesses the neutron spin by  $180^\circ$  about the initial spin direction, thus reversing the sign of the PV spin rotation relative to that due to magnetic fields, indicated in the figure; the counting rate  $(B-A) = 2\phi_{\text{PV}}$ . Figure courtesy of A. Micherdzinska.

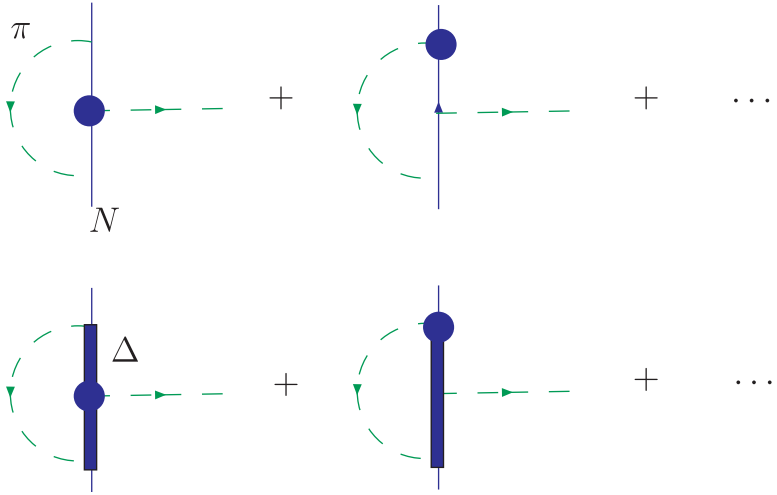


**Figure 11** One-loop contributions to renormalized, parity-violating pion-nucleon Yukawa coupling.